Phytomedicine 135 (2024) 156093

Contents lists available at ScienceDirect

Phytomedicine

journal homepage: www.elsevier.com/locate/phymed

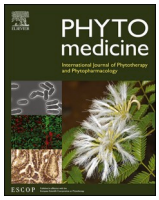

Original Article

Liposomal honokiol inhibits non-small cell lung cancer progression and enhances PD-1 blockade via suppressing M2 macrophages polarization

Yuan Cheng [a,1], Xuejiao Han [a,1], Xintian Lai [b], Xiawei Wei [a,*]

[a] Laboratory of Aging Research and Cancer Drug Target, State Key Laboratory of Biotherapy and Cancer Center, National Clinical Research Center for Geriatrics, Department of Biotherapy, West China Hospital, Sichuan University, Chengdu 610041, Sichuan, People's Republic of China
[b] Chengdu Jinrui Foundation Biotech Co., Ltd, Yizhou Avenue, High Tech Zone, Chengdu 610041, Sichuan, People's Republic of China

ARTICLE INFO

Keywords:
Liposomal Honokiol
Non-small cell lung cancer
Macrophage
PI3K/Akt signal
Immune check-point inhibitor

ABSTRACT

Background: Honokiol (HNK), a natural phenolic compound derived from Magnolia plants, exhibits therapeutic effects on various diseases, including cancer. The advent of immune checkpoint inhibitors (ICIs) has marked a breakthrough in non-small cell lung cancer (NSCLC) treatment. However, a significant subset of patients exhibits primary or acquired resistance to anti-PD-1/PD-L1 therapies, necessitating the development of novel combination strategies to enhance therapeutic efficacy and overcome resistance.

Purpose: This study aimed to explore the anti-tumor efficacy of liposomal honokiol (Lipo-HNK) and elucidate the synergistic effects of Lipo-HNK and ICIs on NSCLC.

Methods: The effects of Lipo-HNK on cell proliferation and apoptosis were assessed in human lung cancer cell lines H460 and A549, and mouse Lewis lung cancer cell line (LL2). A murine lung cancer model was established by injecting LL2 cells via the tail vein to evaluate the therapeutic effects of Lipo-HNK and ICIs. Tumor microenvironment features were characterized using immunofluorescence and flow cytometry. Primary macrophages were extracted from mouse bone marrow for mechanistic studies. High-throughput sequencing and bioinformatics analyses of Lipo-HNK-treated macrophages were conducted to identify key signaling pathways, which were subsequently confirmed by Western blotting and inhibitor blockade.

Results: Lipo-HNK, with enhanced solubility and bioavailability, demonstrated potent cytotoxicity against NSCLC cell lines. In the murine lung cancer model, Lipo-HNK exhibited synergistic anti-cancer effects when combined with anti-PD-1 therapy. Immunofluorescence and flow cytometry analyses revealed that Lipo-HNK significantly reduced the infiltration of myeloid-derived suppressor cells (MDSCs) and M2 macrophages (CD206+). Macrophage depletion experiment showed the anti-tumor effects of Lipo-HNK was macrophage-dependent. M2 macrophages induced by tumor-conditioned medium (TCM) or interleukin-4 (IL-4) released immunosuppressive cytokines such as IL-10, Arg-1, and TGF-β. RNA sequencing analyses showed that Lipo-HNK effectively inhibited the PI3K/Akt signaling pathway, blocking macrophage polarization to the M2 type. Furthermore, the combination of Lipo-HNK and anti-PD-1 therapy led to increased CD8+ *T*-cell infiltration and activation, enhancing the overall anti-tumor immune response.

Conclusion: This study validated the anti-tumor efficacy of Lipo-HNK against NSCLC. Lipo-HNK reduced the infiltration of MDSCs and M2 macrophages by inhibiting the PI3K/Akt pathway and enhanced the therapeutic effects of ICIs. These findings provide evidence and new insights into Lipo-HNK as a promising anti-cancer drug for NSCLC treatment, highlighting its potential to overcome resistance to current ICI therapies.

Abbreviations: Lipo-HNK, liposomal honokiol; NSCLC, non-small cell lung cancer; MDSCs, myeloid-derived suppressor cells; TCM, tumor conditioned medium; ICI, immune check-point inhibitor; LL2, Murine Lewis lung cancer cell line; ICB, immune checkpoint blockade; IC50, half maximal inhibitory concentration; DEGs, differentially expressed genes; PPI, protein-protein interaction networks.

* Corresponding author at: Laboratory of Aging Research and Cancer Drug Target, State Key Laboratory of Biotherapy and Cancer Center, National Clinical Research Center for Geriatrics, Department of Biotherapy, West China Hospital, Sichuan University, No. 17, Block 3, Southern Renmin Road, Chengdu, 610041, Sichuan, People's Republic of China.
E-mail address: xiaweiwei@scu.edu.cn (X. Wei).
[1] These authors contributed equally.

https://doi.org/10.1016/j.phymed.2024.156093
Received 20 May 2024; Received in revised form 31 August 2024; Accepted 23 September 2024
Available online 24 September 2024

Introduction

Cancer remains one of the leading causes of death globally. In 2020, an estimated 19.3 million new cancer cases and almost 10.0 million cancer-related deaths occurred worldwide. Among these, 4.57 million new diagnoses and 3 million deaths occurred in China, ranking it among the highest in the world (Sung et al., 2021). Lung cancer is both the most common cancer type and the leading cause of cancer deaths in China (Zheng, 2022). Although significant advances in cancer therapies have substantially improved patient survival, challenges such as cancer recurrence, drug resistance, and patient heterogeneity complicate the treatment process. The advent of targeted therapy and immunotherapy has revolutionized cancer treatment. With notable achievements, the tremendous investment in immunotherapy has increased the number of active drugs in development from 2030 to 3876, a 91 % increase over a two-year interval (Xin Yu et al., 2019). Novel treatment combinations and newly identified drugs are expected to significantly expand the role of immunotherapy in cancer therapy (Waldman et al., 2020).

Phytomedicine provides new insights into medical preventive and therapeutic approaches. Honokiol (HNK), a natural phenolic compound derived from the bark, seed cones, and leaves of Magnolia trees, has demonstrated anti-inflammatory and antioxidative effects (Rauf et al., 2021). Studies have also shown HNK's potential in anti-tumor therapy. HNK can induce the apoptosis of cancer cells and inhibit their proliferation, leading to tumor regression in tumor xenograft models (Jiang et al., 2008; Zhu et al., 2019a). The mechanisms underlying HNK's anti-tumor potential involve multiple targeted proteins and signaling pathways, including the epidermal growth factor receptor (EGFR), vascular endothelial growth factor (VEGF), JAK-STAT3 signaling pathway, and PI3K/Akt/mTOR signaling pathway (Deng et al., 2019; Fan et al., 2018; Leeman-Neill et al., 2010; Lin et al., 2016; Song et al., 2016). To increase the solubility and absorption of HNK, our lab encapsulated honokiol in liposomes, naming it Lipo-HNK (Wang et al., 2011). We previously found that Lipo-HNK could inhibit the growth of ovarian, lung, and breast cancers both in vitro and in vivo (Hou et al., 2008; Jiang et al., 2008; Li et al., 2008; Luo et al., 2008). Currently, a clinical trial is ongoing in China to investigate the anti-tumor effects of liposomal HNK in patients with NSCLC (Wu et al., 2018).

Immune checkpoint therapy is a major category of cancer immunotherapy, which also includes adoptive cellular therapies and cancer vaccines (Waldman et al., 2020). The aim of immune checkpoint blockade (ICB) is to restore effective T cell function to fight against cancer. Cytotoxic T lymphocyte antigen 4 (CTLA4) and programmed cell death 1 (PD1) are the most well-studied and potent immune checkpoint molecules of T cells (Fife and Bluestone, 2008). Anti-PD-1 drugs can release T cells from a dysfunctional state called T cell exhaustion and rescue $CD8^+$ *T* cell cytotoxicity (Wei et al., 2017). Since Nivolumab was first applied in NSCLC as a second-line treatment, the combination of immunotherapy and chemotherapy has become the standard first-line therapy for patients with NSCLC, regardless of PD-L1 expression levels (Cheng et al., 2021b). Despite the rapid development and success of ICB, the immunosuppressive microenvironment of different tumors makes it difficult to predict which patients will benefit (Ding and Chen, 2019). Myeloid-derived suppressor cells (MDSCs) and tumor-associated macrophages (TAMs) are two major immunosuppressive immune cells in the tumor microenvironment. M2-like TAMs exhibit immunosuppressive properties, suppress $CD8^+$ *T* cell function, and promote the infiltration of Tregs (Xue et al., 2014). Studies have also found a close relationship between M2 macrophage activity and ICB response (Rodell et al., 2018; Zhu et al., 2019b). Elimination of immunosuppressive cells significantly contributes to the increased efficacy of ICB (Loeuillard et al., 2020).

HNK has shown potential in regulating tumor immunity and enhancing anti-tumor immunity (Crane et al., 2009; Zheng et al., 2020). Therefore, this study aims to investigate the synergistic efficacy of Lipo-HNK and anti-PD-1 therapy in lung cancer, and to elucidate the specific mechanisms by which Lipo-HNK regulates tumor immunity. Our findings demonstrate that the combination therapy of Lipo-HNK and anti-PD-1 mAbs exhibits promising anti-tumor effects. The application of Lipo-HNK significantly decreased the infiltration of MDSCs and M2 macrophages in the tumor microenvironment, thereby enhancing the anti-tumor efficacy of ICB. Specifically, Lipo-HNK effectively inhibited the polarization of macrophages to the M2 type by blocking the PI3K/Akt pathway.

Materials and methods

Cell culture and reagents

Murine Lewis lung cancer (LL2), H460 human large cell lung carcinoma, and A549 human non-small-cell lung carcinoma were purchased from the American Type Culture Collection (ATCC). All cells were cultured in Dulbecco's modified Eagle's medium (DMEM, Gibco) supplemented with 10 % fetal bovine serum (FBS), 100 U/ml penicillin, and 100 μg/ml streptomycin in a humidified incubator containing 5 % CO2 at 37 °C.

Reagents and antibodies

Lipo-HNK (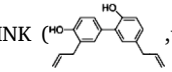 ,with 99.5 % purity) was synthesized and prepared as previously described and kindly provided by Chengdu Jinrui Biotechnology Company (Chengdu, China), with chemical structure (Li et al., 2021; Luo et al., 2008). The lyophilized powder of Lipo-HNK was dissolved in sterilized water and prepared at a concentration of 2 mg/ml for further experiments.

Mouse anti-PD-1 monoclonal antibody (clone RMP1–14, Bio X Cell) and its isotype control antibody (2A3, Bio X Cell) were prepared in phosphate-buffered saline (PBS) at pH 7 and pH 6.5, respectively, according to the manufacturer's instructions.

The antibodies used for western blot analysis and immunohistochemistry were: GAPDH (Cat# 5174), Ki67 (Cat# 12,202), PI3 Kinase α (Cat# 4249), PI3 Kinase β (Cat# 3011), Phospho-Akt (Ser473) (Cat# 4060), Akt (pan) (Cat# 4691) from Cell Signaling Technology (CST), and anti-CD31 (Cat# 28,364) from Abcam. The antibodies for flow cytometry were purchased from Biolegend or BD Biosciences, including CD45, CD11b, F4/80, CD206, IL-10, TGF-β, Arg-1, CD3, CD4, CD8, CD69, Granzyme B, CD44, and Gr-1.

Cell proliferation assay

Cell proliferation was evaluated using the Cell Counting Kit-8 (CCK-8; Dojindo, Kumamoto, Japan). Generally, 2–5 × 10^3 LL2 cells were plated in 96-well plates and incubated with either blank liposome (control) or various concentrations of Lipo-HNK (0–120 μg/ml) for 24 h, 48 h, and 72 h. After treatment, cells were incubated with 10 % CCK-8 reagent for an additional 2 h. The optical density (OD) was measured at 450 nm using a Microplate Reader (Bio-Rad). Cell viability was calculated based on the OD values. The half maximal inhibitory concentration (IC50) values were calculated using GraphPad Prism software.

Cell apoptosis assay

The Annexin V-FITC/propidium iodide (PI) Detection Kit (BD Biosciences) was used to determine the apoptosis rate of H460, A549, and LL2 cells after Lipo-HNK treatment. A total of 5 × 10^5 cells were seeded in 6-well plates and incubated with culture medium in the presence of blank liposome or various concentrations of Lipo-HNK (0, 10, and 20 μg/ml) for 24 h. After 24 h, cells were harvested, washed twice with cold PBS, and stained with Annexin V/PI. The cells were examined using a NovoCyte Flow Cytometer (ACEA Biosciences) within 1 h, and data were analyzed using NovoExpress software (1.3.0, ACEA Biosciences).

Colony formation assay

For the colony formation assay, 500–1000 H460 and A549 cells per well were seeded into 6-well plates and cultured overnight. Different concentrations of Lipo-HNK (10, 20 μg/ml) were added to the culture medium to allow colony formation. After 24 h of treatment, the medium was replaced with fresh DMEM. After one week of culture, the colonies were fixed with cold methanol for 10 min and stained with 0.5 % crystal violet (Beyotime Institute of Biotechnology, China) for 10 min. After several washes, the colonies were photographed. The LL2 cell line was not included in the colony formation assay due to its characteristic loose attachment or floating in the medium.

Mice

Female C57BL/6 wild-type mice (6–8 weeks old, weighing 18–22 g) were purchased from Vital River (Beijing, China). The mice were housed and maintained under specific-pathogen-free (SPF) conditions with consistent room temperature and humidity. All animal experiments were performed according to the guidelines of the Institutional Animal Care and Use Committee of Sichuan University (Chengdu, Sichuan, China), and protocols were approved by the Institutional Animal Care and Use Committee of Sichuan University.

Tumor challenge and treatment experiments

In the in vivo experiments, 6–7 female C57BL/6 mice were used in each group. For the subcutaneous tumor model, 100 μl of cell suspension containing 5 × 10^5 LL2 cells were injected subcutaneously into the right flank, and treatment was started when the tumors became palpable (generally 5 days after tumor implantation). For the metastatic lung cancer model, 100 μl of cell suspension containing 2 × 10^5 LL2 cells were injected intravenously through the tail vein, and treatment was started on day 5. Based on our pilot experiment results and other similar research, Lipo-HNK was intravenously injected at a concentration of 20 mg kg^{-1} every 2 days until the end of the experiment (Cheng et al., 2011). Meanwhile, the 4-dose intraperitoneal injection of anti-PD-1 mAb (10 mg kg^{-1}) started on the same day as the first Lipo-HNK injection. Clodronate liposomes (200 μl, FormuMax Scientific, F70101C-A) were administered by tail vein injection on days 1, 8, 15 and 22 (control liposomes were used as a control) for macrophage depletion experiment. Tumor volume was monitored every three days and calculated as length × width^2 × 1/2. Mice were sacrificed on days 25–30, and tumors and lungs were harvested, weighed, and photographed.

Flow cytometry analysis

The lungs containing tumor nodules were collected after the mice were sacrificed. Mouse lung tissues were dissected, cut into small pieces, and digested into single-cell suspensions using 1 mg/ml collagenase Type I, 0.5 mg/ml Type IV, and 10 μg/ml DNase I in RPMI 1640 basic medium for 1 hour at 37 °C. Red blood cells (RBCs) were lysed using RBC lysis buffer (154 mM NH4Cl, 10 mM KHCO3, 0.1 mM EDTA, pH 7.4). The LIVE/DEAD™ Fixable Near-IR Dead Cell Stain Kit (L34975, Thermo Fisher Scientific) was used to exclude dead cells. Cells were counted, dispersed in PBS at 1 × 10^6 cells/ml, and stained with 1 μl of fluorescence-conjugated antibodies for 30 min in 100 μl PBS at 4 °C in the dark. For intracellular staining, cells were fixed and permeabilized using BD Cytofix/Cytoperm™ solution (BD Biosciences) according to the manufacturer's protocol. All samples were collected on a NovoCyte Flow Cytometer (ACEA Biosciences) and analyzed using NovoExpress software (1.3.0, ACEA Biosciences).

H&E staining and immunohistochemistry

Lung tissues containing tumor nodules were embedded in 4 % methanol-free formaldehyde for 48 h. Subsequently, the tumor nodules in lung tissues were assessed in 4 μm-thick hematoxylin and eosin (H&E)-stained sections. To evaluate tumor angiogenesis and proliferation, the expression of CD31 and Ki67 was assessed by staining with anti-CD31 mAb and anti-Ki67 mAb. Images of H&E staining and immunohistochemistry were obtained under a light microscope.

Bone marrow-derived macrophages (BMDMs) isolation and polarization

Bone marrow cells were harvested from the femurs and tibias of C57BL/6 mice (6–8 weeks old) by flushing the bone cavities using culture medium without FBS and filtering through a 70 μm nylon mesh, followed by RBC lysis. The cells were cultured in DMEM containing 10 % FBS and 20 ng/ml of mouse Macrophage Colony-Stimulating Factor (M-CSF) (R&D Systems) with 5 % CO2 at 37 °C for 5–7 days to induce BMDMs. BMDMs were stimulated with 20 ng/ml mouse IL-4 (Pepro-Tech) for 24 h to polarize to the M2 type. For the polarization inhibition experiment, Lipo-HNK (10 μg/ml) was added to the medium for 30 min before IL-4 treatment.

T cell suppression study

Spleens were harvested from 8-week-old female C57BL/6 wild-type mice and gently pressed through a 70 μm cell strainer to obtain a single-cell suspension. The resulting suspension was resuspended in 4–5 ml of lymphocyte separation medium (Dakewe, China) and subjected to gradient centrifugation at 800 g for 30 min. Purified lymphocytes were then labeled with CFSE (Invitrogen) to monitor cell proliferation. These CFSE-labeled lymphocytes were cultured in 24-well plates containing complete RPMI medium. Pre-treated macrophages (at a 1:1 ratio) was added to the wells for co-culture experiment. After a 72-hour incubation, T cells were harvested and analyzed for proliferation and IFN-γ production.

High-throughput sequencing and bioinformatics analysis

After 24 h of treatment with IL-4 (20 ng/ml) or in combination with Lipo-HNK (10 μg/ml), BMDMs were harvested for total RNA isolation, with three biological replicates for each group. Pearson's correlation coefficients and principal component analysis (PCA) were applied to test the quality of the biological replicates. Genes expressed in at least one sample were defined as detected genes. A log2 (fold change) > 1 or < -1 with p-value < 0.05 was defined as the threshold for differentially expressed genes (DEGs). Gene functions were annotated using the Kyoto Encyclopedia of Genes and Genomes (KEGG, C2.cp.kegg.v6.2) and Gene Ontology (GO, C6.all.v6.2) enrichment analysis. Hierarchical clustering and heatmap analysis with the limma R package (v 3.38.3) assessed the differential gene set enrichment (cutoff of $p < 0.05$).

Western blot analysis

BMDMs were stimulated with the indicated treatments for 24 h, and total cellular proteins were extracted using RIPA lysis buffer containing a protease inhibitor cocktail (Biosharp). The bicinchoninic acid assay (BCA) protein assay kit (Thermo Fisher Scientific) was used to quantify protein concentrations. Equal amounts of protein samples were loaded and separated by SDS-PAGE gels and transferred onto polyvinylidene fluoride (PVDF) membranes (Millipore). After blocking the membranes with 5 % milk dissolved in Tris-buffered saline with 0.1 % Tween-20 (TBS-T) for 1 hour at room temperature, the membranes were incubated at 4 °C overnight with antibodies against PI3 Kinase α, PI3 Kinase β, Phospho-Akt (Ser473), Akt, and GAPDH. After incubation with the appropriate secondary HRP-conjugated antibodies, the protein expressions were detected by enhanced chemiluminescence (ECL) using SuperSignal West Pico Plus Chemiluminescent Substrate (Thermo Fisher Scientific). GAPDH was used as a loading control.

RNA extraction and quantitative real-time PCR

Reverse transcription polymerase chain reaction (RT-PCR) was used to measure mRNA transcription levels of Arg-1, PD-1, and PD-L1 expressed by macrophages. Total RNA was extracted using an RNA isolation kit (Foregene, Chengdu, China). The RNA was reverse-transcribed into cDNA using the PrimeScript RT reagent kit (TaKaRa, Japan). Primers used were: 5′-CAAGAATGGAAGAGTCAG-3′ and 5′-ATATGCAGGGAGTCACC-3′ for mouse Arg-1, 5′-GCAAT-CAGGGTGGCTTCT-3′ and 5′-TTGGCTCAAACCATTACAGA-3′ for mouse PD-1, 5′-CTGCTTGCGTTAGTGGTGTA-3′ and 5′-GCGTGATTCGCTTG-TAGTCC-3′ for mouse PD-L1, and 5′-ACCCAGAAGACTGTGGATGG-3′ and 5′-CACATTGGGGGTAGGAACAC-3′ for mouse GAPDH. Real-time PCR was performed using SYBR Green supermix (Bio Rad) with a two-step PCR reaction procedure. Expression of the genes was normalized to the expression of GAPDH. Data were analyzed using the $2^{-\Delta\Delta Ct}$ method.

Statistical analysis

Statistical analyses were performed using GraphPad Prism 8 software (GraphPad Prism, San Diego, CA, USA) and presented as mean ± SEM. Differences between two groups were analyzed using a two-tailed unpaired Student's *t*-test, whereas multiple groups were compared using ANOVA. Results were considered statistically significant at $p < 0.05$.

Result

Lipo-HNK inhibited cell proliferation and induced apoptosis in lung cancer cells

The preparation and molecular characteristics of Lipo-HNK have been described in our previous study (Luo et al., 2008). To investigate the anti-tumor effects of Lipo-HNK on lung cancer, we conducted CCK8 assays on two human lung cancer cell lines (H460 and A549) and the murine Lewis lung carcinoma cell line (LL2), treating them with Lipo-HNK at concentrations ranging from 0 to 120 μg/ml for 24, 48, and 72 h. As shown in Fig. 1a, the cell viability of lung cancer cells decreased with increasing concentrations of Lipo-HNK. The dose-dependent cytotoxicity was not prominent at both low and high concentrations. Due to the varying sensitivity among different cell lines, the effective concentrations ranged from 10 to 60 μg/ml. The half-maximal inhibitory concentration (IC50) for the three cell lines is presented in Fig. 1b, showing a decrease in IC50 with longer treatment times. The anti-tumor effect of Lipo-HNK demonstrated a dose-dependent manner within the effective concentration range; however, the time dependency was not significant. During the cell viability assays, noticeable apoptosis was observed in all tested lung cancer cells treated with Lipo-HNK. Annexin V-FITC/PI staining was performed to assess apoptosis post-treatment. Both early-phase (Annexin *V*+/PI-) and late-phase (Annexin *V*+/PI+) apoptotic cells were considered as apoptotic. Flow cytometric analysis after 24-hour treatment with Lipo-HNK or liposomes revealed that Lipo-HNK significantly induced apoptosis in lung cancer cells. The apoptotic rates for LL2, H460, and A549 increased from 8.9 %, 6.4 %, and 6.3 % to 25.7 %, 36.4 %, and 20.0 %, respectively (Blank vs. 20 μg/ml) (Fig. 1c and d). Colony formation assays for H460 and A549 further confirmed the inhibitory effects of Lipo-HNK (Fig. 1e). These results suggest that Lipo-HNK shows promise as a potential anti-cancer agent due to its sensitivity in lung cancer cells.

Lipo-HNK suppressed lung cancer growth and showed synergistic effects with PD-1 blockade therapy in vivo

The anti-cancer effects of Lipo-HNK have been demonstrated in various mouse models in several studies (Jiang et al., 2008; Li et al., 2008; Luo et al., 2008). Given that anti-PD-1 therapy is a promising approach in cancer immunotherapy, but often with limited efficacy as monotherapy, we evaluated the combined effects of Lipo-HNK and anti-PD1 monoclonal antibody (RMP1–14, BioXCell) in LL2 tumor-bearing C57BL/6 mice (Fig. 2a). Both subcutaneous and metastatic lung cancer models were treated with vehicle, Lipo-HNK (20 mg kg^{-1}, i.v., every 2 days), anti-PD1 antibody (10 mg kg^{-1}, i.p., every 5 days), or the combination of Lipo-HNK and anti-PD1 antibody (Fig. 2b). Lipo-HNK treatment alone led to reduced tumor growth in the subcutaneous tumor model, and the combination therapy was more effective than either monotherapy (Fig. 2c). At the experimental endpoint, the tumor volume in the combination group was approximately 576.3 mm^3, while the volumes in the PD-1, Lipo-HNK, and NS groups were 1196 mm^3, 922.18 mm^3, and 1428.3 mm^3, respectively. The tumor weight in the combination group was also the smallest, around 0.482 g, compared to 1.16 g, 0.816 g, and 1.526 g in the PD-1, Lipo-HNK, and NS groups, respectively (Fig. 2d and e). The growth rate and tumor size were significantly inhibited by the combination therapy. In the metastatic lung cancer model, Lipo-HNK combined with anti-PD1 therapy demonstrated notable therapeutic effects (Fig. 2f). The number of tumor nodules in the lungs was significantly reduced in the combination therapy group compared to the vehicle or monotherapy groups (Fig. 2g). Total lung weights were also lighter in the combination therapy group (Fig. 2h). Control treatments with blank liposomes and isotype 2A3 did not show significant effects on tumor progression (Supplementary Figure 1). Immunohistochemical analysis of CD31 and Ki67 in the lung tissue from the metastatic lung cancer model validated Lipo-HNK's potential to inhibit tumor proliferation and vascularization (Fig. 2i). In both the Lipo-HNK monotherapy and combination therapy groups, the positive proportions of CD31 and Ki67 were significantly decreased.

Lipo-HNK significantly reduced immunosuppressive cells infiltration and promoted T cells activation in tumors

To explore the mechanisms underlying the synergistic anti-tumor effects of Lipo-HNK and anti-PD1 combination therapy, we analyzed immune cell infiltration in the tumor microenvironment using flow cytometry. Myeloid-derived suppressor cells (MDSCs) and immunosuppressive macrophages (M2 macrophages) were characterized as $CD45^+CD11b^+Gr1^+$ and $CD45^+CD11b^+F4/80^+CD206^+$, respectively (Fig. 3a). Results showed that M2 macrophages and MDSCs were significantly reduced in both the Lipo-HNK monotherapy and combination therapy groups, indicating that Lipo-HNK may inhibit the infiltration of immunosuppressive cells into the tumor microenvironment (Fig. 3b and Supplementary Figure 2). M2 macrophages contribute to an immunosuppressive microenvironment that supports tumor growth. To elucidate the mechanisms by which Lipo-HNK inhibits macrophage polarization, primary macrophages were isolated from mice for further analysis. Immunofluorescence analysis of lung tissues from tumor-bearing mice revealed a significant reduction in M2 macrophages ($F4/80^+CD206^+$) in Lipo-HNK treated groups, including both monotherapy and combination therapy groups (Fig. 3c). Furthermore, clodronate liposomes was used to deplete macrophages in vivo (control liposome as control), aiming to validate the role of macrophage in the anti-cancer effects of Lipo-HNK (Chen et al., 2023; Li et al., 2022a). The peak effect of clodronate liposomes was observed 24 h post-injection and persisted for at least 5 days or longer. Clodronate liposomes (200 μl) via tail vein on days 1, 7, 14 and 21, while LL2 cells injected subcutaneously on day 0. Animals were sacrificed on day 25. Lipo-HNK (20 mg kg^{-1}, i.v., every 2 days) exhibited anti-cancer effects in the control liposome group; however, these effects were not significant in the clodronate liposome group (Fig. 3d). After clodronate liposome treatment, Lipo-HNK was unable to effectively inhibit tumor growth (Fig. 3e). Following macrophage depletion, there was no significant difference in tumor size and weight between the Lipo-HNK and NS groups (Fig. 3f and g). On the other hand, we observed that macrophage depletion with clodronate liposomes directly slowed tumor growth (Fig. 3e-g).

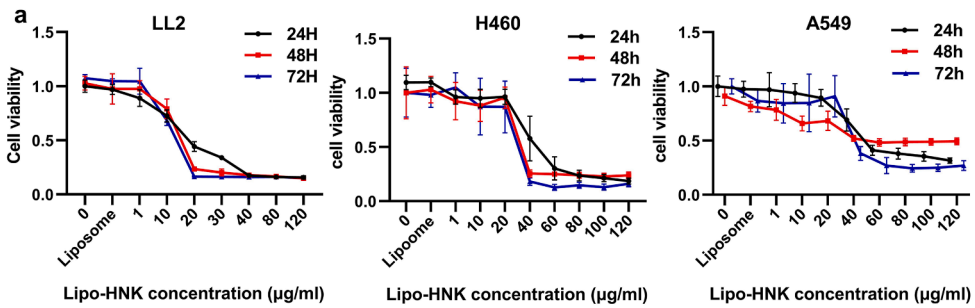

b

Cell lines	IC50 (μg/ml)		
	24h	48h	72h
LL2	18.5	14.8	12.0
H460	38.8	27.7	24.0
A549	42.2	36.5	33.1

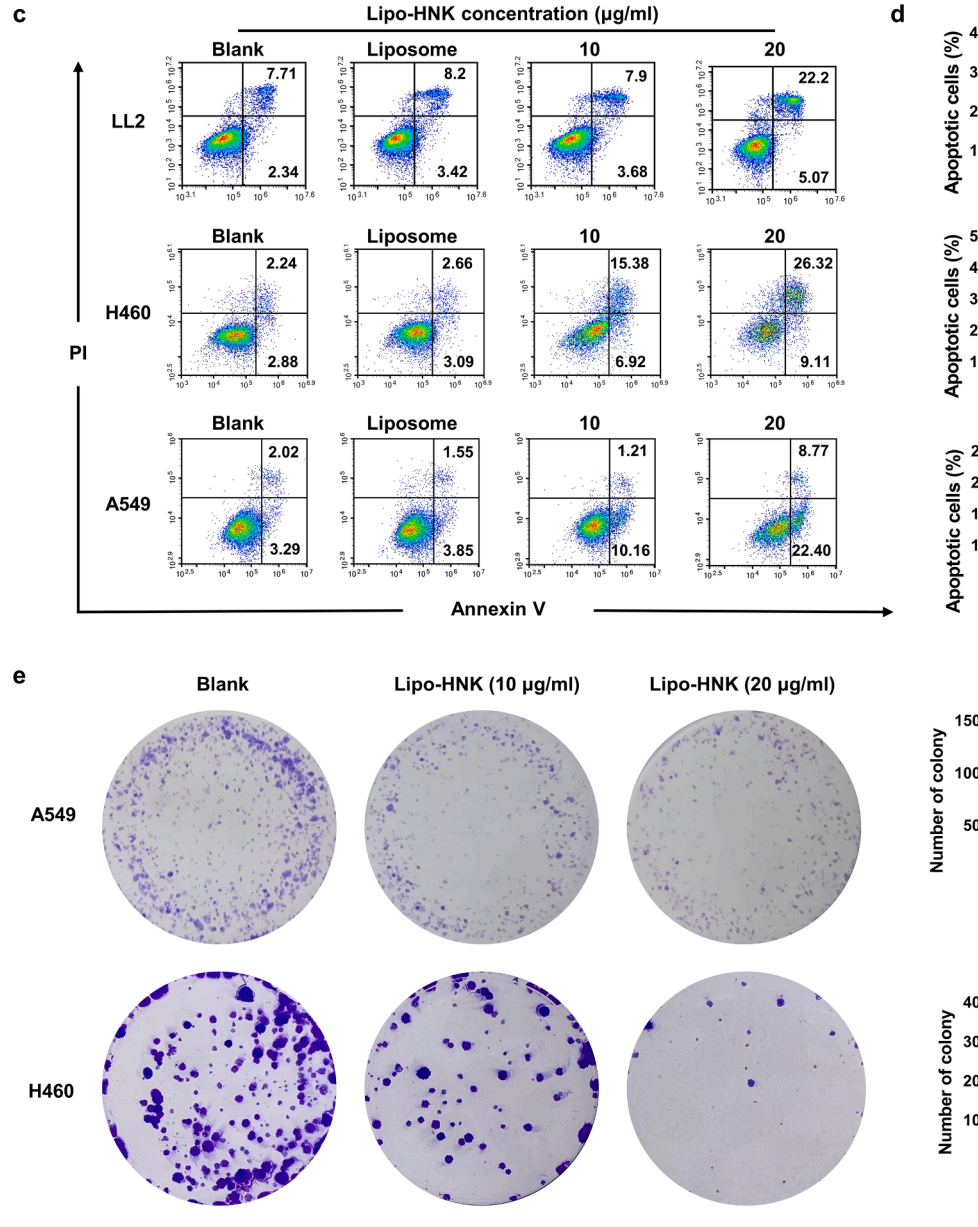

Fig. 1. Lipo-HNK inhibits cell proliferation and induces apoptosis in lung cancer cells. (a-b) CCK8 proliferation assay of LL2, H460, and A549 cells treated by escalating doses of Lipo-HNK (0–120 μg/ml) for 24 h, 48 h, and 72 h (a) and corresponding IC50 concentration of Lipo-HNK (b). Data was shown as mean ± SEM. (c-d) Flow cytometric analyses of apoptotic LL2, H460, and A549 cells. Lung cancer cells were treated by different concentration of Lipo-HNK (0, 10, and 20 μg/ml) for 24 h and stained with PI-Annexin V (c). Annexin *V*+/PI− and Annexin *V*+/PI+ were both considered apoptotic. Statistic results of apoptotic cell assay (d). Data was shown as mean ± SEM, $n = 3$. (e) Colony formation assay of H460 and A549 cells. After 24-h Lipo-HNK (0, 10, and 20 μg/ml) treatment, cells were cultured for another 7 days with fresh medium. Colonies were visualized by crystal violet staining (left) and counted (right). Data was shown as mean ± SEM, $n = 3$. $^{*}p < 0.05$, $^{**}p < 0.01$, $^{***}p < 0.001$, ns represents $p > 0.05$.

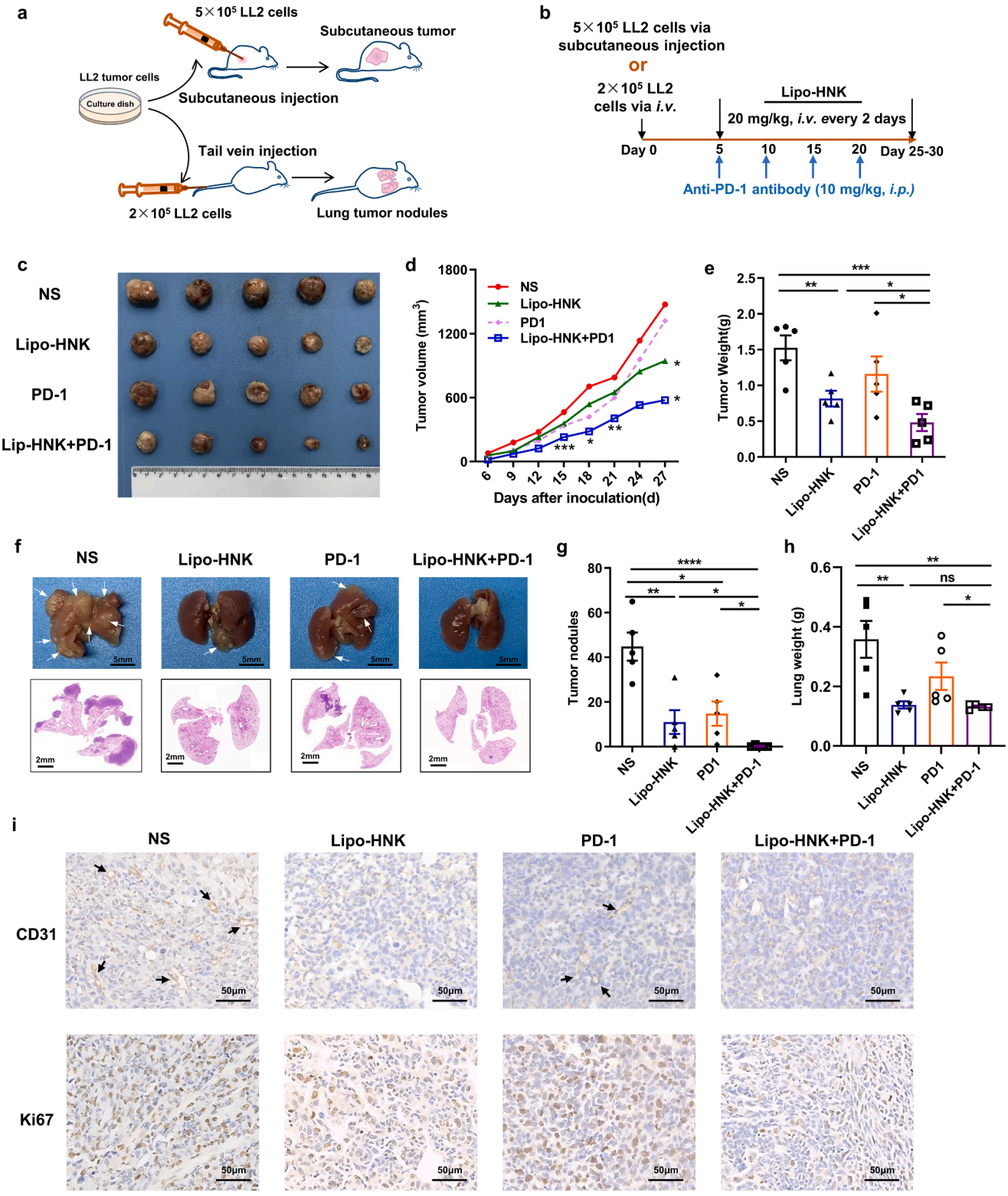

Fig. 2. Lipo-HNK suppresses lung cancer growth and showed synergistic effects with PD-1 blockade therapy in vivo. (a) Construction of subcutaneous tumor model and metastatic lung cancer model in mice, $n = 6–7$. For subcutaneous tumor model, 5×10^5 LL2 cells were injected into the right flank of C57BL/6 mice. For metastatic lung cancer model, 2×10^5 LL2 cells were injected into tail vein of C57BL/6 mice. (b) Therapy regimen of the mice model experiment. Lipo-HNK and Anti-PD-1 antibody were administered at 20 mg kg^{-1} by intravenous injection and 10 mg kg^{-1} by intraperitoneal injection(i.p.), respectively. The mice were sacrificed and the tumor or pulmonary nodules was evaluated. $n = 6–7$. (c) Tumors from subcutaneous tumor model at the end point of experiment. (d-e) Tumor growth curves and tumor weight at the sacrifice of subcutaneous tumor model. Data was shown as mean ± SD. (f) Lung tissues with tumor nodules and H&E staining from metastatic lung cancer model. $n = 6–7$. (g-h) Measurement of total lung weight and metastatic tumor nodules from metastatic lung cancer model, Data was shown as mean ± SD. (i) Immunohistochemistry staining of vascular markers CD31 and proliferation marker Ki67 in the lung tissue of mice from metastatic lung cancer model group. Scale bar, 50 μm. $^*p < 0.05$, $^{**}p < 0.01$, $^{***}p < 0.001$, ns represents $p > 0.05$.

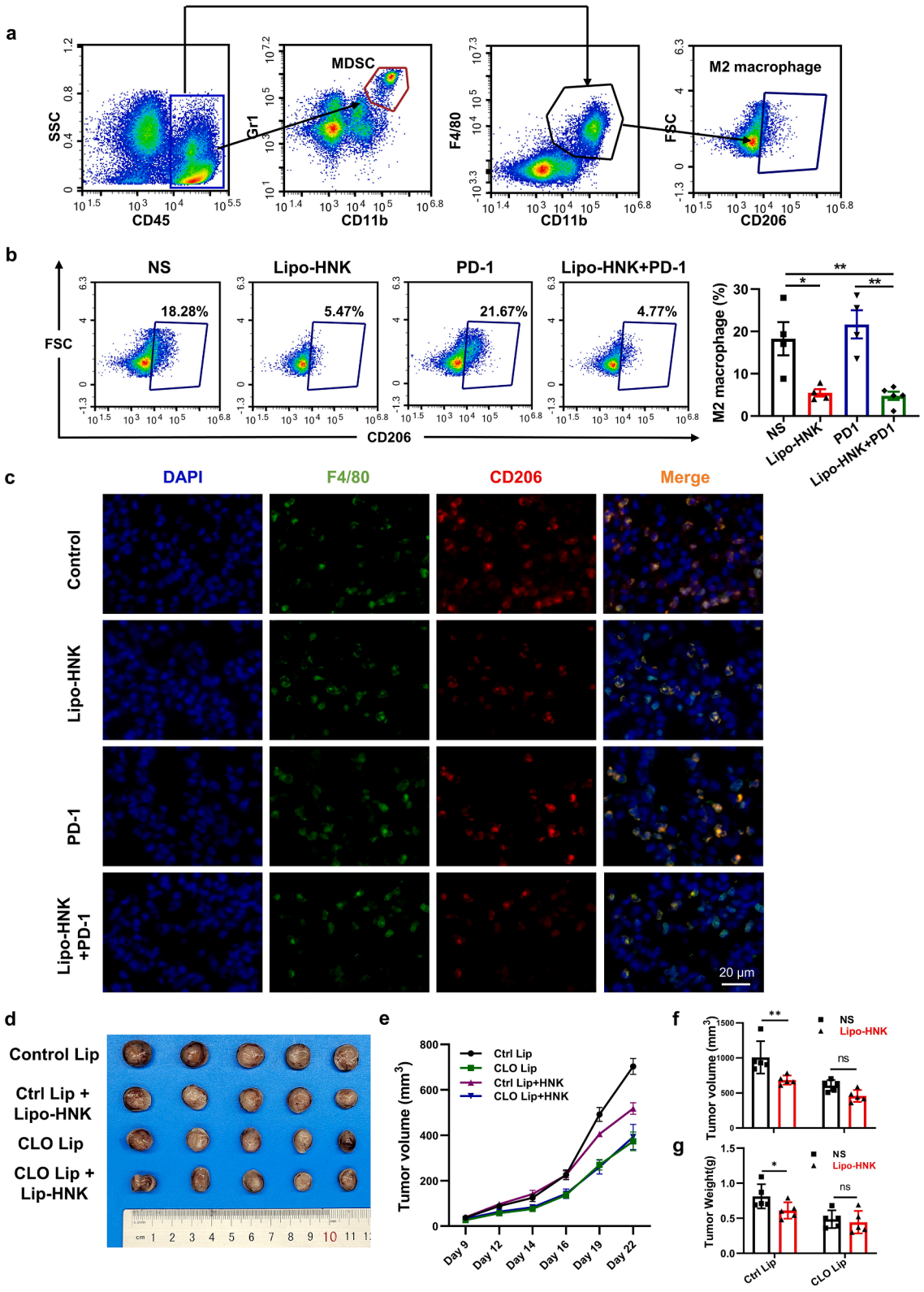

Fig. 3. Lipo-HNK inhibits tumor growth by reducing the infiltration of M2 macrophages. (a) Flow cytometric characterization of Myeloid-derived suppressor cell (MDSC, $CD45^{+}CD11b^{+}Gr1^{+}$) and M2-macrophage ($CD45^{+}CD11b^{+}F4/80^{+}CD206^{+}$) from tumor tissues. (b) M2 macrophages infiltrated in the tumor microenvironment of mice in metastatic lung cancer model (left) and quantification of infiltrated immune cells (right). Data was shown as mean ± SEM, $n = 6$–7. (c) Immunofluorescence analysis of M2 macrophages infiltration in the tumor tissues of mice in metastatic lung cancer model. M2 macrophages were labelled as F4/80- and CD206-positive. Green, F4/80; red, CD206; blue, DAPI. (d-i) C57BL/6 mice were injected with LL2 on Day 0 ± clodronate liposomes (200 μl) via tail vein on days 1, 7, 14 and 21. Control liposomes was given as control. The subcutaneous tumors at day 25 after LL2 cell injection (d). The tumor growth curve (e), tumor volume (f) and weights (g) of subcutaneous tumors were recorded. Data are expressed as mean ± SEM. $^{*}p < 0.05$, $^{**}p < 0.01$, $^{***}p < 0.001$, ns represents $p > 0.05$.

In vitro experiment, primary macrophages were then treated with IL-4 (20 ng/ml), tumor-conditioned medium (TCM), Lipo-HNK (10 μg/ml), or their combinations. Flow cytometric analyses showed that macrophages were activated by IL-4 and TCM, polarizing towards the M2 phenotype, but Lipo-HNK treatment significantly inhibited this polarization (Supplementary Figure 3a). Further, Lipo-HNK treatment also significantly reduced the levels of key cytokines secreted by M2 macrophages, including IL-10, Arg-1, and TGF-β (Supplementary Figure 3b-d). These findings validate the efficacy of Lipo-HNK in inhibiting macrophage polarization towards the M2 phenotype and the anti-tumor effects of Lipo-HNK was dependent on macrophages.

Lipo-HNK promotes T cell activation in tumors

T cell response plays a critical role in anti-tumor immunity, particularly in anti-PD1 immunotherapy. In our study, we found activated $CD8^+$ *T* cells ($CD8^+CD69^+$), effector $CD8^+$ *T* cells ($CD8^+$Granzyme B^+), and memory $CD4^+$ *T* cells ($CD4^+CD44^+$) were significantly increased in the Lipo-HNK plus anti-PD1 combination therapy group, with only slight increases in the monotherapy groups (Fig. 4a-d). Other T cell subsets, including activated $CD4^+$ *T* cells and memory $CD8^+$ *T* cells, remained unchanged (Supplementary Figure 4). Activation of $CD8^+$T cells can exert direct anti-tumor effects. We further examined the activation status of $CD8^+$T cells in tumor tissues using immunofluorescence staining. The results showed a higher number of activated CD8 T cells in the group treated with the combination of PD-1 antibody and Lipo-HNK (Fig. 4e). Macrophages can function as antigen-presenting cells to activate T cells, while M2 macrophages, in contrast, inhibit $CD8^+$T cell activation. Given that we have already demonstrated Lipo-HNK's ability to reduce M2 macrophage infiltration, we conducted in vitro experiments where macrophages were polarized into the M2 phenotype using IL-4, and this polarization was blocked by Lipo-HNK. We found that IL-4-induced M2 macrophages inhibited T cell proliferation (Fig. 4g), reduced T cell activation (Fig. 4h), and decreased IFN-γ secretion by T cells (Fig. 4i). The addition of Lipo-HNK counteracted the effects of IL-4, promoting T cell proliferation and activation. These findings demonstrate that Lipo-HNK enhances T cell activation by reducing M2 macrophage infiltration, thereby exerting anti-tumor effects, which may play a critical role in the synergistic anti-tumor effects observed with anti-PD1 therapy

Analysis of differentially expressed genes (DEGs) using high-throughput sequencing

To elucidate the molecular mechanisms underlying Lipo-HNK's effects on macrophage polarization, we conducted high-throughput sequencing and bioinformatics analyses to explore transcriptomic alterations induced by Lipo-HNK treatment. Primary macrophages were treated with IL-4 (20 ng/ml) alone or in combination with Lipo-HNK (10 μg/ml) for 24 h, followed by bioinformatic analysis. The correlation plot and principal component analysis (PCA) demonstrated high reproducibility, with biological replicates closely grouped (Supplementary Figure 5). Cluster analysis revealed over 800 genes that were differentially expressed following IL-4 treatment (data not shown). The DEGs ($p < 0.05$) shared among the blank, IL-4, and IL-4+Lipo-HNK groups are presented in Fig. 5a.

To identify key genes or signaling pathways involved in Lipo-HNK's effects on macrophage polarization, we used a Venn diagram to identify unique and shared genes (differential expression > |2-fold) across four groups: Blank vs IL-4_up, Blank vs IL-4_down, and IL-4 vs IL-4+Lipo-HNK_up (Fig. 5b). We observed that IL-4 treatment led to a slight predominance of up-regulated over down-regulated genes in macrophages. However, Lipo-HNK treatment primarily down-regulated gene expression in IL-4 treated macrophages (Supplementary Figure 6a). Volcano plot and protein-protein interaction (PPI) network analyses further confirmed that Lipo-HNK was more strongly associated with down-regulation of genes in IL-4 treated macrophages (Supplementary Figure 6b and c).

Based on these observations, DEGs shared between the Blank vs IL-4_up and IL-4 vs IL-4+Lipo-HNK_down groups were selected for further analysis. The Venn diagram identified six DEGs (Gpr183, Stard13, Serpinb2, Cd69, Nyap2, and Col12a1) shared between these two groups. Additionally, two DEGs (Gpr150, Dennd3) were shared between the Blank vs IL-4_down and IL-4 vs IL-4+Lipo-HNK_up groups. KEGG pathway enrichment analysis of the Blank vs IL-4 and IL-4 vs IL-4+Lipo-HNK groups revealed the top 20 altered pathways (Fig. 5c and d). Several pathways, including proteoglycans in cancer, protein digestion and absorption, ECM-receptor interaction, PI3K-Akt signaling, and platelet activation, were shared between the two groups. Both KEGG pathway enrichment and DEG clustering analyses suggested that the PI3K-Akt signaling pathway is likely involved in IL-4-induced M2 macrophage polarization and the inhibitory effects of Lipo-HNK on this process (Supplementary Figure 7b). Gene ontology (GO) enrichment analysis further identified the top 20 GO terms associated with DEGs, which are presented in Supplementary Figure 7b.

Lipo-HNK suppressed M2 macrophages polarization via PI3K/Akt signaling pathway

The PI3K/Akt signaling pathway has been implicated in macrophage activation (Zhao et al., 2020). IPI549, a selective inhibitor of PI3K-γ with over 58-fold selectivity against other PI3K isoforms (PI3Kα, PI3Kβ, and PI3Kδ), can effectively block the PI3K/Akt signaling pathway (Evans et al., 2016). Primary macrophages were treated with IPI549 (1 μM) for 30 min before IL-4 (20 ng/ml) was added to the medium. Flow cytometric analysis showed that IPI549 partially blocked IL-4-induced M2 macrophage polarization (Fig. 6a).

To investigate the relationship between Lipo-HNK and the PI3K/Akt pathway, we performed Western blot analysis. IL-4 treatment effectively activated the PI3K/Akt pathway, whereas Lipo-HNK treatment reduced PI3K expression and Akt phosphorylation (Fig. 6b and c). To further validate the inhibitory effects of Lipo-HNK on M2 macrophage polarization, we applied 740 Y-P, an agonist of the PI3K/Akt signaling pathway, in subsequent experiments. Lipo-HNK was confirmed to block M2 macrophage polarization, but 740 Y-P induced re-polarization towards the M2 phenotype (Fig. 6d). Additionally, Lipo-HNK reduced the expression of immunosuppressive markers in macrophages, including Arg-1, PD-1, and PD-L1, while re-activation of the PI3K/Akt pathway restored these markers' expression levels (Fig. 6e and f). These findings suggest that the down-regulation of PD-1 and PD-L1 expression by Lipo-HNK could be a potential mechanism underlying the synergy observed with anti-PD-1 therapy. Collectively, these results demonstrate that the PI3K/Akt pathway plays a critical role in Lipo-HNK's inhibitory effects on M2 macrophage polarization.

Discussion

Natural products and their structural analogues have played a crucial role in drug discovery, particularly in the treatment of cancer and infectious diseases (Atanasov et al., 2015; Mann, 2002). Herbs and plants naturally contain a variety of active compounds and are increasingly considered as alternative treatment options for various diseases (Harvey et al., 2015). Honokiol, an active compound derived from Magnolia officinalis, has demonstrated promising anti-tumor effects across multiple cancer types, including glioma, lung cancer, breast cancer, nasopharyngeal carcinoma, and leukemia (Fan et al., 2018; Yang et al., 2017a; Zhang et al., 2013; Zhou et al., 2017; Zhu et al., 2019a). In this study, we found that Lipo-HNK, a liposomal formulation of honokiol synthesized in our laboratory, effectively inhibited lung cancer growth both in vitro and in vivo (Luo et al., 2008; Wang et al., 2011). Lipo-HNK induced apoptosis and inhibited the proliferation of lung cancer cells in vitro. Furthermore, the combination of Lipo-HNK with anti-PD-1

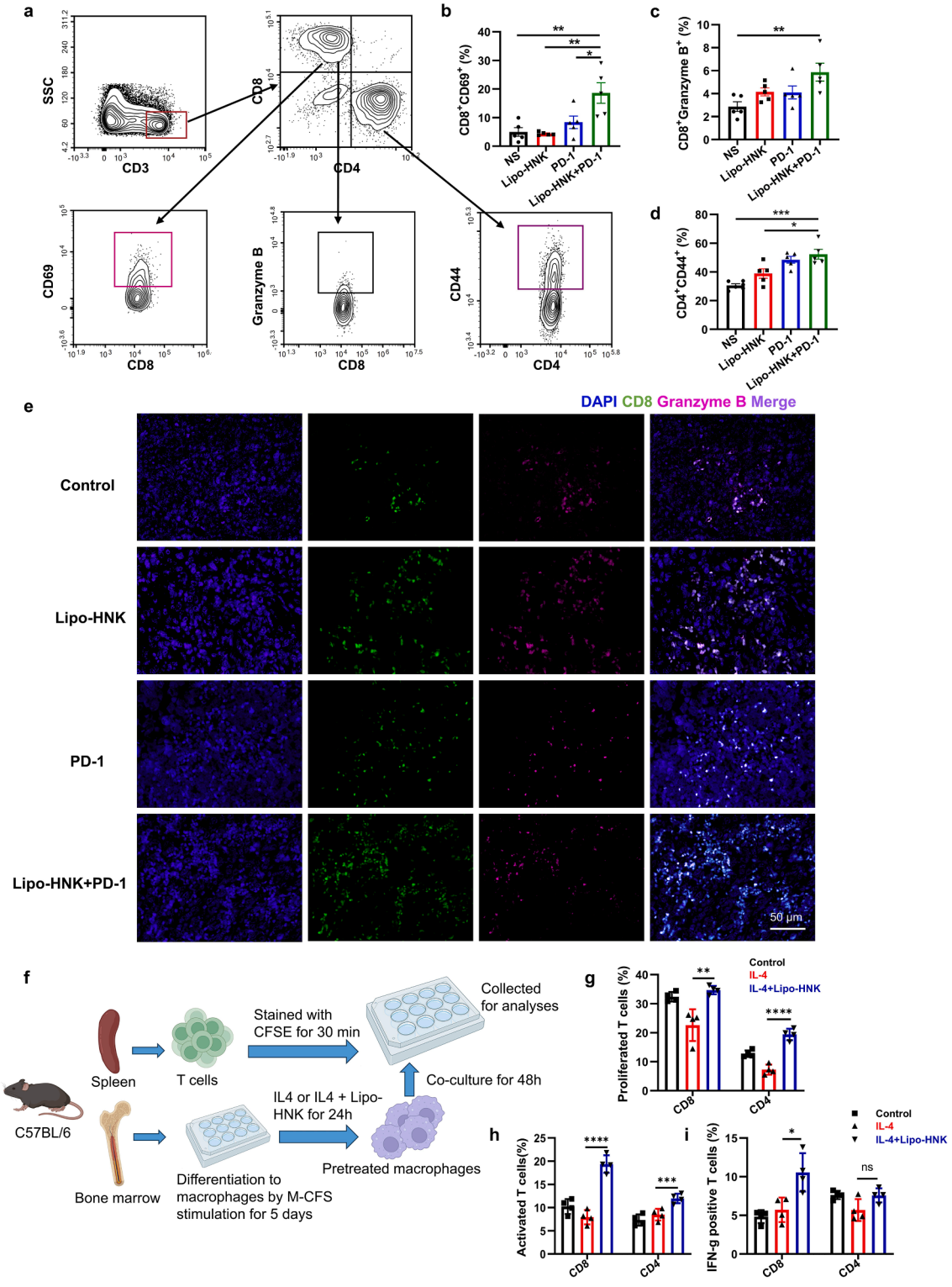

Fig. 4. Lipo-HNK promotes T cell activation in tumors. (a) Flow cytometric characterization of activated CD8-positive T cells ($CD3^+CD8^+CD69^+$or $CD3^+CD8^+$Granzyme B^+) and memory CD4-positive T cells ($CD3^+CD4^+CD44^+$) from tumor tissues. (b-d) Statistic results of flowcytometric analyses Data are expressed as mean ± SD. (e) Immunofluorescence analysis of activated $CD8^+$ *T* cells infiltration in the tumor tissues of mice in subcutaneous tumor model. Activated $CD8^+$ *T* cells were labelled as CD8- and Granzyme B-positive. Green, CD8; Pink, Granzyme B; blue, DAPI. (f) BMDMs were extracted from the femurs of healthy C57BL/6 mice and then induced by M-CSF (20 ng/ml) for 5 days. IL-4 (20 ng/ml) with or without Lipo-HNK (20 μg/ml) was added in the culture medium for 24 h to get pre-treated macrophages. Primary T lymphocytes were extracted from the spleen of healthy mice, stained with CFSE, and then co-cultured with pre-treated macrophages for another 48 h. The T cells were harvested for flow cytometric analyses. (g-i) Quantification of T cell proliferation rate (CFSE, g), activated rate ($CD69^+$, h), and IFN-g production (i) were analyzed. Data are expressed as mean ± SD. CFSE, carboxy fluorescein diacetate succinimidyl ester. $^*p < 0.05$, $^{**}p < 0.01$, $^{***}p < 0.001$, ns represents $p > 0.05$.

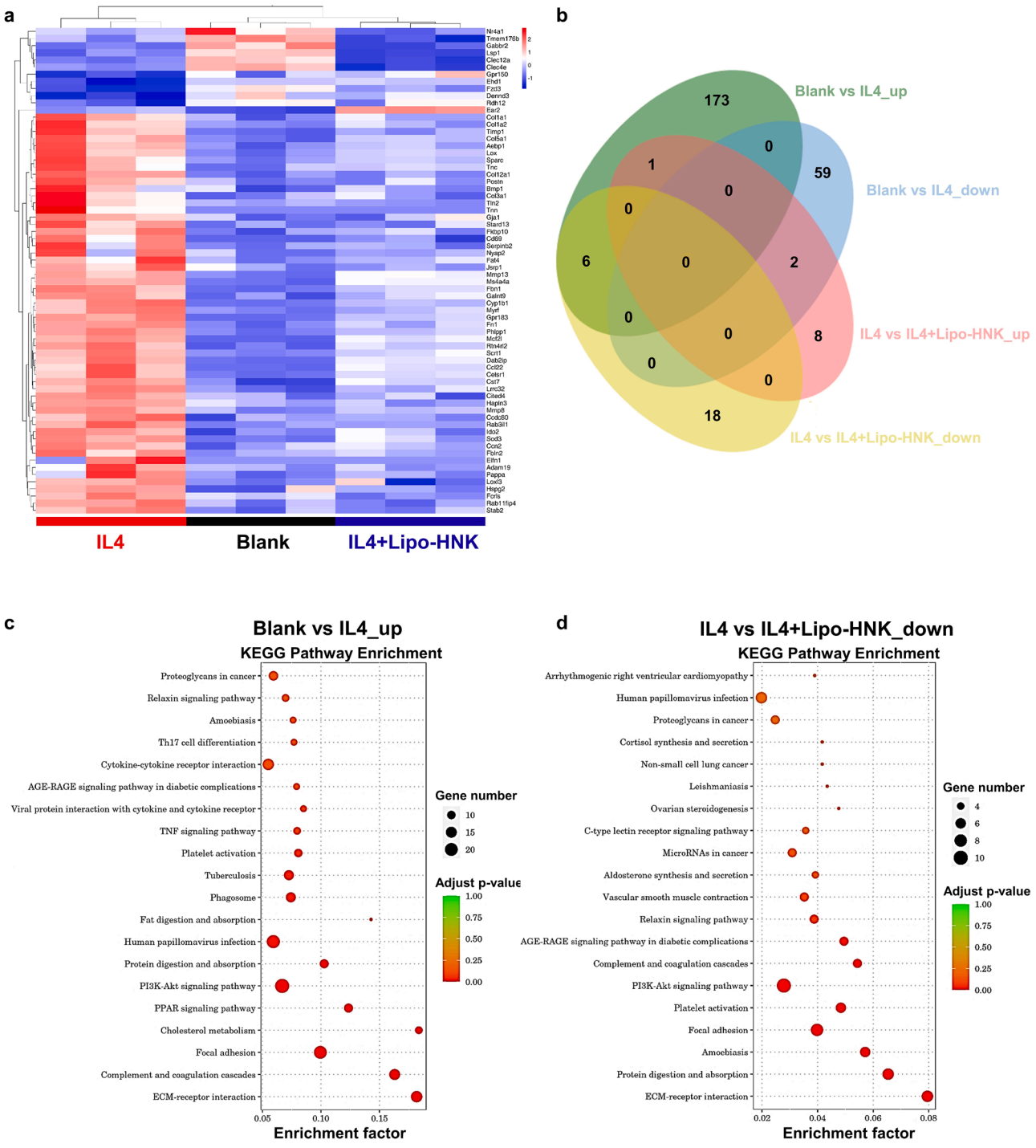

Fig. 5. Expression of differentially expressed genes was analyzed by high-throughput sequencing and KEGG pathway analysis. Macrophages isolated from bone marrow were treated by IL4 (20 ng/ml) or in combination with Lipo-HNK (10 μg/ml) for 24 h and collected for high-throughput sequencing. (a) Heatmap analysis comparing transcript abundances quantitated by sequencing reads in transcripts per million (TPM) data of significantly changed genes among blank, IL4, and IL-4+Lipo-HNK groups. (b) Venn diagram depicting unique and shared gene families identified in four groups: Blank vs IL4_up, Blank vs IL4_down, IL4 vs IL4+Lipo-HNK_up, and IL4 vs IL4+Lipo-HNK_down. Blank vs IL4_up was referred to genes up-regulated after IL-4 treatment. (c-d) KEGG pathway analysis of differentially expressed genes enriched in Blank vs IL4_up (c) and IL4 vs IL4+Lipo-HNK_down (d). Y-axis label represents pathway, and X-axis label represents enrichment factor. The size and color of the bubble represented the amount of differentially expressed genes enriched in the pathway and enrichment significance, respectively.

monoclonal antibodies (mAbs) exhibited synergistic anti-tumor efficacy in mouse models of subcutaneous and lung metastatic tumors. Lipo-HNK was well-tolerated and showed potent anti-tumor activity, not only by directly killing tumor cells but also by modulating the tumor microenvironment. Notably, Lipo-HNK treatment increased the population of activated CD8+ *T* cells and memory CD4+ *T* cells, while decreasing the infiltration of immunosuppressive cells such as myeloid-derived suppressor cells (MDSCs) and M2 macrophages. Mechanistic investigations using bioinformatics analyses identified the PI3K/Akt signaling pathway as a key mechanism underlying Lipo-HNK's inhibitory effects on M2 macrophage polarization (Fig. 7). By identifying the PI3K/Akt signaling pathway as a mechanism through which Lipo-HNK exerts these effects,

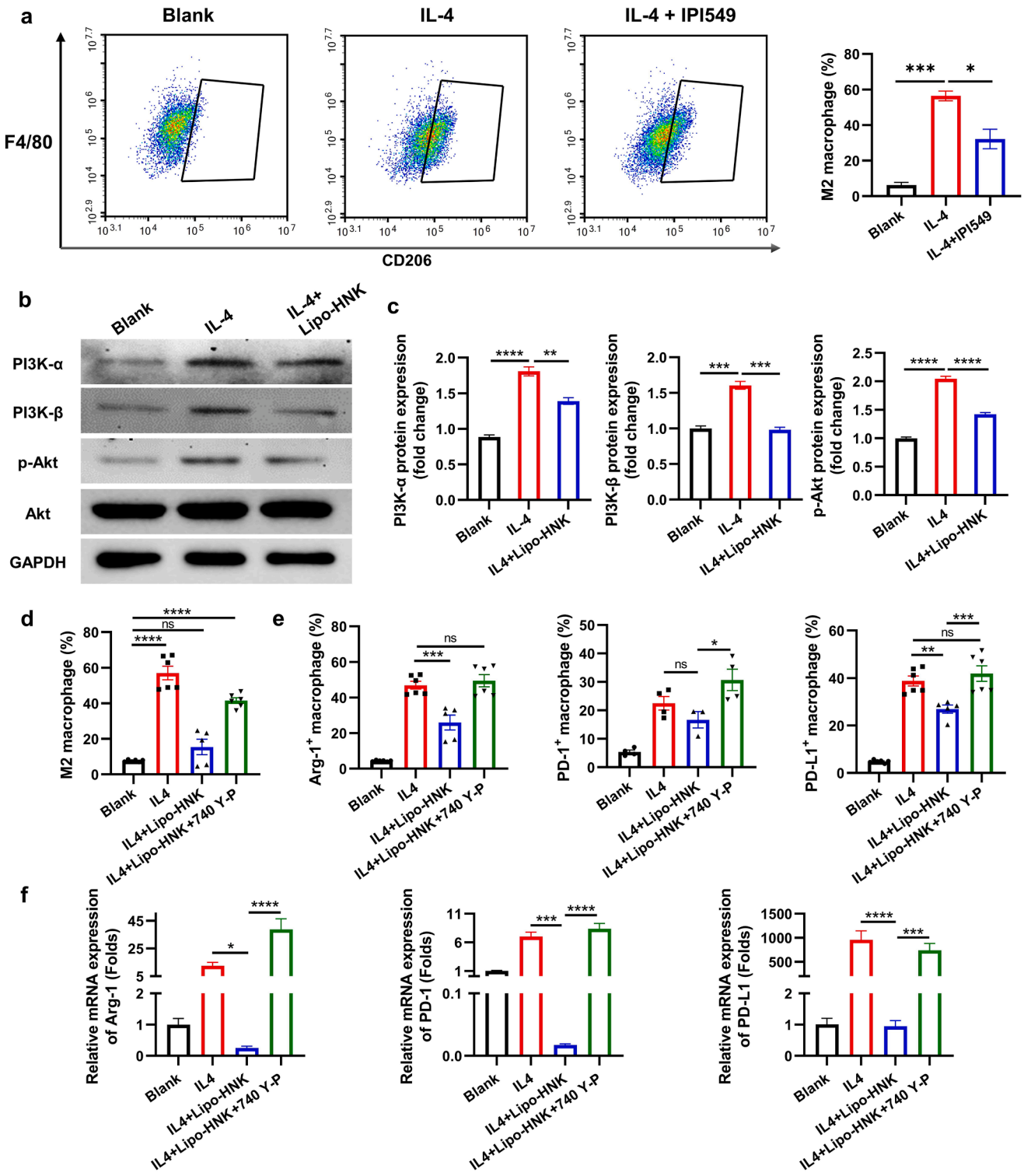

Fig. 6. Lipo-HNK suppressed M2 macrophages polarization via PI3K/Akt signaling pathway. (a) Flowcytometric analyses of M2 macrophage polarization. Macrophages were treated with IL-4 (20 ng/ml) or in combination with IPI549 (1 μM) for 24 h. Data was shown as mean ± SEM. (b-c) Western blot analyses of PI3K/Akt signaling pathway in macrophages treated by IL-4 (20 ng/ml) or in combination with Lipo-HNK (10 μg/ml). GAPDH was used as a loading control (b). Protein expression levels were qualified by densitometry analysis using ImageJ software (c). Data was shown as mean ± SEM. (d) Flowcytometric analyses of M2 macrophage polarization and the expression of Arg-1, PD-1, and PD-L1 in macrophages. Macrophages were treated with IL-4 (20 ng/ml) or in combination with Lipo-HNK (10 μg/ml) and activator of PI3K (740 Y-P, 5 μM) for 24 h. Data was shown as mean ± SEM. (e) qPCR analyses of mRNA levels of Arg-1, PD-1, and PD-L1 in (d). Data was shown as mean ± SEM. $^{*}p < 0.05$, $^{**}p < 0.01$, $^{***}p < 0.001$, ns represents $p > 0.05$.

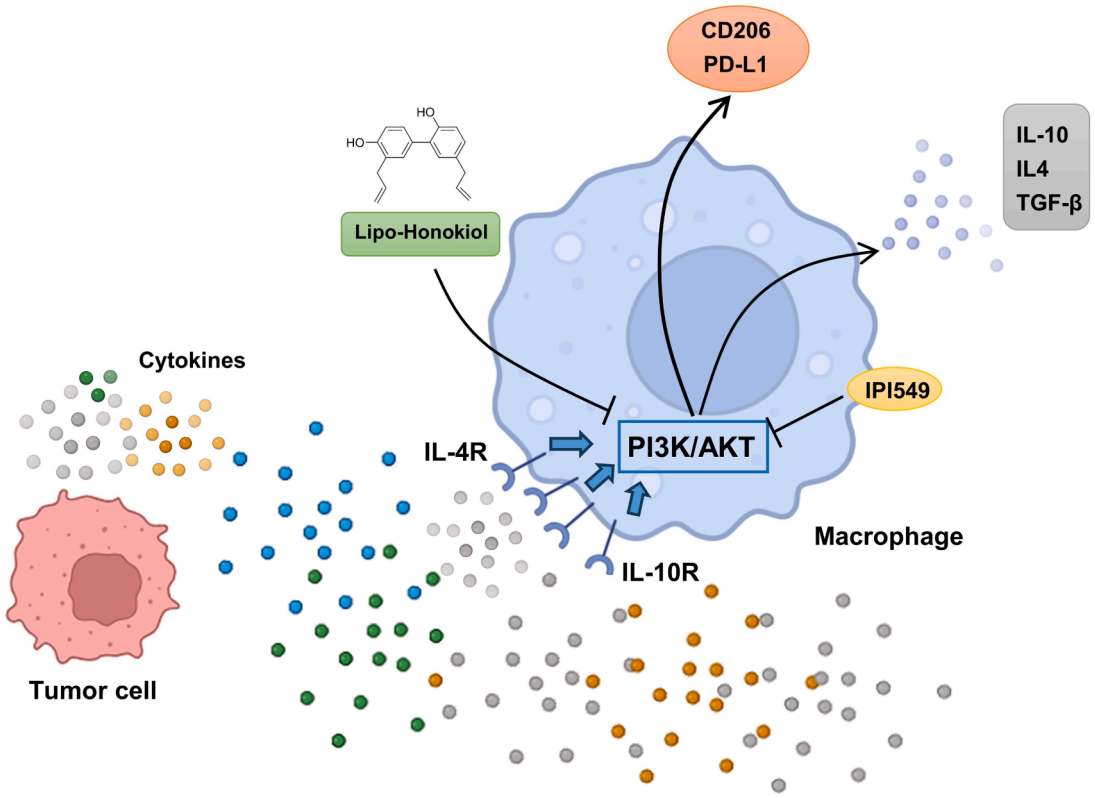

Fig. 7. Lipo-HNK reduces M2 macrophage polarization by inhibiting the activation of the PI3K/AKT pathway. Various cytokines in the tumor microenvironment, such as IL-4 and IL-10, can induce macrophage polarization by activating the PI3K/AKT pathway, leading to the polarization of M0 macrophages into the pro-tumorigenic M2 subtype. M2 macrophages are characterized by increased surface expression of CD206 and PD-L1 and secrete immunosuppressive cytokines like IL-10, IL-4, and TGF-β, thereby promoting tumor progression. Our study found that Lipo-HNK could inhibit the activation of the PI3K/AKT pathway, reducing the presence of M2 macrophages in the tumor microenvironment, and consequently, suppressing tumor growth.

our study provides a mechanistic basis for targeting TME in combination therapies for anticancer treatment.

As the active component of *Magnolia officinalis*, honokiol has been widely used in traditional Chinese medicine for various applications, including anti-infective, anti-depressive, and anti-tumor treatments (Rauf et al., 2021). Recent studies have uncovered the therapeutic potential of honokiol in treating neurological disorders due to its ability to cross the blood-brain barrier and regulate mitochondrial function (Zhou et al., 2023). Lipo-HNK (JRF101, Honokiol Liposome for Injection) has been reviewed and approved by the U.S. Food and Drug Administration (FDA) this year, aiming to evaluate the clinical safety, tolerability, and pharmacokinetics of JRF101 in patients with advanced malignant solid tumors. Our study validates the anti-tumor effects of Lipo-HNK in both in vitro and in vivo models and explores new mechanistic directions. Specifically, our research delves into the modulation of macrophage polarization by Lipo-HNK through the PI3K/Akt signaling pathway, highlighting a novel mechanism by which Lipo-HNK exerts its anti-tumor effects. Previous studies have also highlighted honokiol's potential as a combination or adjuvant therapy in cancer treatment. For instance, liposomal Honokiol has demonstrated significant anti-tumor effects in human medulloblastoma, highlighting its potential as a promising therapeutic agent for this aggressive type of brain cancer. The ability of liposomal formulations to enhance the bioavailability and efficacy of Honokiol by improving its delivery to tumor sites while minimizing systemic toxicity is particularly noteworthy (Li et al., 2022b). Honokiol has been shown to induce lysosomal degradation of Hsp90 client proteins, leading to the death of gefitinib-resistant non-small cell lung cancer (NSCLC) cells (Yang et al., 2017b). Additionally, the combination of Lipo-HNK and radiotherapy produced synergistic anti-tumor effects in a murine lung cancer model (Hu et al., 2008). Our lab has previously demonstrated that combining Lipo-HNK with cytotoxic chemotherapy yields promising synergistic anti-tumor efficacy in several cancer types (Hou et al., 2008; Jiang et al., 2008). Honokiol also exhibits potent anti-angiogenic and anti-lymphangiogenic properties in tumor models (Ma et al., 2011; Wen et al., 2009). Importantly, recent studies have underscored honokiol's potential in modulating the tumor immune microenvironment. Honokiol-treated tumor cell lysates, acting as damage-associated molecular patterns (DAMPs), enhanced dendritic cell (DC) maturation and T cell activation (Jiraviriyakul et al., 2019; Klingensmith et al., 2018). Honokiol treatment significantly increased the expression of pro-inflammatory cytokines such as IL-1β and TNF-α (Chen et al., 2017), and inhibited the immunosuppression caused by ultraviolet (UV) radiation (Prasad et al., 2017). Honokiol has shown significant potential in immunomodulation, particularly in regulating immune responses within the tumor microenvironment. Our study provides a detailed elucidation of the PI3K/Akt pathway's role in Lipo-HNK's modulation of macrophage polarization, highlighting its importance in shifting macrophages from a tumor-promoting M2 phenotype to a tumor-suppressing state. These findings underscore honokiol's ability to regulate the immune microenvironment within tumors.

Immunotherapy has emerged as a cornerstone of cancer treatment, with immune checkpoint blockade (ICB) being one of the most promising and rapidly developing approaches (Morad et al., 2021). Anti-PD-1/PD-L1 immunotherapy is now a standard treatment for patients with advanced-stage NSCLC (Reck et al., 2022). However, not all patients respond to immunotherapy, highlighting the need for combination therapies to expand the applicability of ICB (Huang et al., 2021). Programmed cell death protein 1 (PD-1) is expressed on activated T cells, natural killer (NK) cells, and myeloid cells (Hsu et al., 2018; Nam

et al., 2019), while its ligands, PD-L1 and PD-L2, are primarily expressed on tumor and myeloid cells (Bianchini et al., 2019; Gibbons Johnson and Dong, 2017). The interaction between PD-1 and its ligands suppresses T cell function and is a major mechanism of tumor immune evasion, characterized by reduced activation of $CD8^+$ *T* cells (Hirano et al., 2005; Iwai et al., 2002). In our study, we found that the combination of Lipo-HNK with anti-PD-1 mAbs restored $CD8^+$ *T* cell activation, as evidenced by increased expression of CD69 and Granzyme B. Lipo-HNK treatment also enhanced the population of memory $CD4^+$ *T* cells ($CD44^+$), which have been implicated in anti-tumor responses (Zheng et al., 2008).

The immunosuppressive environment within tumor tissues presents a significant challenge to the broader application of immunotherapy. Studies have shown that the low response rate to immune checkpoint blockade (ICB) therapy is largely due to the immunosuppressive environment within tumor tissues. This environment, characterized by the presence of regulatory T cells, myeloid-derived suppressor cells (MDSCs), and M2 macrophages, inhibits the activation and function of effector T cell (Binnewies et al., 2018). Immune cells within the tumor microenvironment can influence the tumor's response to ICB, either suppressing or promoting tumor progression. MDSCs and macrophages are two types of myeloid cells with immunosuppressive activity (Boutilier and Elsawa, 2021; Dysthe and Parihar, 2020). MDSCs express high levels of PD-L1 and produce immunosuppressive cytokines across various cancer types, thereby impairing T cell function (Lu et al., 2016). Elimination of MDSCs has been shown to enhance T cell activation and inhibit tumor growth (Cheng et al., 2021a; Retseck et al., 2018). Moreover, studies have found that MDSCs and M2-like macrophages mediate resistance to ICB in certain tumors (Kim et al., 2019; Yu et al., 2021). Reducing the presence of MDSCs and tumor-associated macrophages has been shown to improve the anti-tumor efficacy of ICB (Loeuillard et al., 2020). In our study, we observed that Lipo-HNK significantly reduced the infiltration of MDSCs and M2 macrophages in tumor tissues, consistent with findings from other studies (Mihara et al., 2017). In vitro experiments revealed that Lipo-HNK decreased the expression of PD-1 and PD-L1 on macrophages. PD-1 expression on macrophages has been associated with reduced phagocytic activity against tumor cells (Gordon et al., 2017; Strauss et al., 2020).

Furthermore, our study confirmed the inhibitory effect of Lipo-HNK on the polarization of macrophages to the M2 phenotype. Honokiol has been shown to suppress the activation of the NLRP3 inflammasome in renal resident macrophages, alleviating lupus nephritis (Ma et al., 2023). Additionally, Lipo-HNK has been reported to regulate macrophage polarization by activating STAT1 and inhibiting STAT6 signaling, resulting in glioblastoma regression (Li et al., 2021). In the current study, we identified the PI3K/Akt signaling pathway as the major mechanism through which Lipo-HNK regulates macrophage polarization and function. Lipo-HNK treatment inhibited the PI3K/mTOR pathway in tumor tissues without impairing T cell function (Crane et al., 2009). The PI3K/Akt/mTOR pathway is a critical signaling pathway involved in macrophage activation and M1/M2 polarization (Vergadi et al., 2017). Specifically, PI3K activation is closely associated with M2 macrophage polarization in response to surfactant protein A or IL-4 (Weisser et al., 2011). Targeting the PI3K/Akt pathway in tumors has also been found to synergistically enhance the anti-tumor efficacy of ICB (Liu et al., 2022). Given the evidence of Lipo-HNK's role in tumor immunology, it is evident that Lipo-HNK plays a significant role in regulating macrophage function. Lipo-HNK treatment significantly inhibited macrophage polarization to the M2 phenotype by blocking the PI3K/Akt signaling pathway.

The anti-tumor effects and immune-modulating abilities of Lipo-HNK have been explored in several studies. In this study, we provide novel insights and evidence supporting the combination of Lipo-HNK with anti-PD-1 mAbs. In conclusion, Lipo-HNK suppresses tumor growth by inhibiting the proliferation and inducing apoptosis of lung cancer cells. Given honokiol's ability to modulate the tumor microenvironment, the combination of Lipo-HNK with anti-PD-1 mAbs exhibited synergistic anti-tumor effects in lung cancer models. Specifically, Lipo-HNK effectively inhibited M2 macrophage polarization and modulated macrophage function by blocking the PI3K/Akt pathway. Current evidence positions Lipo-HNK as a promising anti-tumor agent and adjuvant therapy for cancer treatment. Further investigation into combination therapies involving Lipo-HNK is warranted.

CRediT authorship contribution statement

Yuan Cheng: Writing – original draft, Visualization, Validation, Methodology, Investigation, Formal analysis, Data curation. **Xuejiao Han:** Writing – original draft, Validation, Methodology, Investigation, Data curation. **Xintian Lai:** Supervision, Resources, Methodology. **Xiawei Wei:** Writing – review & editing, Validation, Supervision, Project administration, Conceptualization.

Declaration of competing interest

The authors declare the following financial interests/personal relationships which may be considered as potential competing interests: Xintian Lai works for Chengdu Jinrui Foundation Biotech Co., Ltd, which provided liposomal honokiol for this study. Other authors declared no conflict interest.

Funding

This work was supported by the National Natural Science Foundation of China (82102896), Natural Science Foundation of Sichuan Province (2024NSFSC1883), Post-Doctor Research Project, West China Hospital, Sichuan University (2024SCU12022), and Post-doctor Research Fund of West China Hospital, Sichuan University (2024HXBH055).

Supplementary materials

Supplementary material associated with this article can be found, in the online version, at doi:10.1016/j.phymed.2024.156093.

References

Atanasov, A.G., Waltenberger, B., Pferschy-Wenzig, E.M., Linder, T., Wawrosch, C., Uhrin, P., Temml, V., Wang, L., Schwaiger, S., Heiss, E.H., Rollinger, J.M., Schuster, D., Breuss, J.M., Bochkov, V., Mihovilovic, M.D., Kopp, B., Bauer, R., Dirsch, V.M., Stuppner, H., 2015. Discovery and resupply of pharmacologically active plant-derived natural products: a review. Biotechnol. Adv. 33, 1582–1614.

Bianchini, M., Duchene, J., Santovito, D., Schloss, M.J., Evrard, M., Winkels, H., Aslani, M., Mohanta, S.K., Horckmans, M., Blanchet, X., Lacy, M., von Hundelshausen, P., Atzler, D., Habenicht, A., Gerdes, N., Pelisek, J., Ng, L.G., Steffens, S., Weber, C., Megens, R.T.A., 2019. PD-L1 expression on nonclassical monocytes reveals their origin and immunoregulatory function. Sci. Immunol. 4.

Binnewies, M., Roberts, E.W., Kersten, K., Chan, V., Fearon, D.F., Merad, M., Coussens, L. M., Gabrilovich, D.I., Ostrand-Rosenberg, S., Hedrick, C.C., Vonderheide, R.H., Pittet, M.J., Jain, R.K., Zou, W., Howcroft, T.K., Woodhouse, E.C., Weinberg, R.A., Krummel, M.F., 2018. Understanding the tumor immune microenvironment (TIME) for effective therapy. Nat. Med. 24, 541–550.

Boutilier, A.J., Elsawa, S.F., 2021. Macrophage polarization states in the tumor microenvironment. Int. J. Mol. Sci. 22.

Chen, S., Wang, M., Lu, T., Liu, Y., Hong, W., He, X., Cheng, Y., Liu, J., Wei, Y., Wei, X., 2023. JMJD6 in tumor-associated macrophage regulates macrophage polarization and cancer progression via STAT3/IL-10 axis. Oncogene 42, 2737–2750.

Chen, X., Hu, Y., Shan, L., Yu, X., Hao, K., Wang, G.X., 2017. Magnolol and honokiol from Magnolia officinalis enhanced antiviral immune responses against grass carp reovirus in Ctenopharyngodon idella kidney cells. Fish Shellfish Immunol. 63, 245–254.

Cheng, N., Xia, T., Han, Y., He, Q.J., Zhao, R., Ma, J.R., 2011. Synergistic antitumor effects of liposomal honokiol combined with cisplatin in colon cancer models. Oncol. Lett. 2, 957–962.

Cheng, Y., Mo, F., Li, Q., Han, X., Shi, H., Chen, S., Wei, Y., Wei, X., 2021a. Targeting CXCR2 inhibits the progression of lung cancer and promotes therapeutic effect of cisplatin. Mol. Cancer 20, 62.

Cheng, Y., Zhang, T., Xu, Q., 2021b. Therapeutic advances in non-small cell lung cancer: focus on clinical development of targeted therapy and immunotherapy. MedComm 2, 692–729 (2020).

Crane, C., Panner, A., Pieper, R.O., Arbiser, J., Parsa, A.T., 2009. Honokiol-mediated inhibition of PI3K/mTOR pathway: a potential strategy to overcome immunoresistance in glioma, breast, and prostate carcinoma without impacting T cell function. J. Immunother. 32, 585–592.
Deng, S., Zhang, C., Yang, L., Ma, L., 2019. Formylated honokiol analogs showed antitumor activity against lung carcinoma. Anticancer Drugs 30, 795–802.
Ding, L., Chen, F., 2019. Predicting tumor response to PD-1 blockade. N. Engl. J. Med. 381, 477–479.
Dysthe, M., Parihar, R., 2020. Myeloid-derived suppressor cells in the tumor microenvironment. Adv. Exp. Med. Biol. 1224, 117–140.
Evans, C.A., Liu, T., Lescarbeau, A., Nair, S.J., Grenier, L., Pradeilles, J.A., Glenadel, Q., Tibbitts, T., Rowley, A.M., DiNitto, J.P., Brophy, E.E., O'Hearn, E.L., Ali, J.A., Winkler, D.G., Goldstein, S.I., O'Hearn, P., Martin, C.M., Hoyt, J.G., Soglia, J.R., Cheung, C., Pink, M.M., Proctor, J.L., Palombella, V.J., Tremblay, M.R., Castro, A.C., 2016. Discovery of a selective phosphoinositide-3-kinase (PI3K)-gamma inhibitor (IPI-549) as an immuno-oncology clinical candidate. ACS Med. Chem. Lett. 7, 862–867.
Fan, Y., Xue, W., Schachner, M., Zhao, W., 2018. Honokiol eliminates glioma/glioblastoma stem Cell-Like cells via JAK-STAT3 signaling and inhibits tumor progression by targeting epidermal growth factor receptor. Cancers (Basel) 11.
Fife, B.T., Bluestone, J.A., 2008. Control of peripheral T-cell tolerance and autoimmunity via the CTLA-4 and PD-1 pathways. Immunol. Rev. 224, 166–182.
Gibbons Johnson, R.M., Dong, H., 2017. Functional expression of programmed death-ligand 1 (B7-H1) by immune cells and tumor cells. Front. Immunol. 8, 961.
Gordon, S.R., Maute, R.L., Dulken, B.W., Hutter, G., George, B.M., McCracken, M.N., Gupta, R., Tsai, J.M., Sinha, R., Corey, D., Ring, A.M., Connolly, A.J., Weissman, I.L., 2017. PD-1 expression by tumour-associated macrophages inhibits phagocytosis and tumour immunity. Nature 545, 495–499.
Harvey, A.L., Edrada-Ebel, R., Quinn, R.J., 2015. The re-emergence of natural products for drug discovery in the genomics era. Nat. Rev. Drug Discov. 14, 111–129.
Hirano, F., Kaneko, K., Tamura, H., Dong, H., Wang, S., Ichikawa, M., Rietz, C., Flies, D. B., Lau, J.S., Zhu, G., Tamada, K., Chen, L., 2005. Blockade of B7-H1 and PD-1 by monoclonal antibodies potentiates cancer therapeutic immunity. Cancer Res. 65, 1089–1096.
Hou, W., Chen, L., Yang, G., Zhou, H., Jiang, Q., Zhong, Z., Hu, J., Chen, X., Wang, X., Yuan, Y., Tang, M., Wen, J., Wei, Y., 2008. Synergistic antitumor effects of liposomal honokiol combined with adriamycin in breast cancer models. Phytother. Res. 22, 1125–1132.
Hsu, J., Hodgins, J.J., Marathe, M., Nicolai, C.J., Bourgeois-Daigneault, M.C., Trevino, T. N., Azimi, C.S., Scheer, A.K., Randolph, H.E., Thompson, T.W., Zhang, L., Iannello, A., Mathur, N., Jardine, K.E., Kirn, G.A., Bell, J.C., McBurney, M.W., Raulet, D.H., Ardolino, M., 2018. Contribution of NK cells to immunotherapy mediated by PD-1/PD-L1 blockade. J. Clin. Invest. 128, 4654–4668.
Hu, J., Chen, L.J., Liu, L., Chen, X., Chen, P.L., Yang, G., Hou, W.L., Tang, M.H., Zhang, F., Wang, X.H., Zhao, X., Wei, Y.Q., 2008. Liposomal honokiol, a potent anti-angiogenesis agent, in combination with radiotherapy produces a synergistic antitumor efficacy without increasing toxicity. Exp. Mol. Med. 40, 617–628.
Huang, M.Y., Jiang, X.M., Wang, B.L., Sun, Y., Lu, J.J., 2021. Combination therapy with PD-1/PD-L1 blockade in non-small cell lung cancer: strategies and mechanisms. Pharmacol. Ther. 219, 107694.
Iwai, Y., Ishida, M., Tanaka, Y., Okazaki, T., Honjo, T., Minato, N., 2002. Involvement of PD-L1 on tumor cells in the escape from host immune system and tumor immunotherapy by PD-L1 blockade. Proc. Natl. Acad. Sci. USA 99, 12293–12297.
Jiang, Q.Q., Fan, L.Y., Yang, G.L., Guo, W.H., Hou, W.L., Chen, L.J., Wei, Y.Q., 2008. Improved therapeutic effectiveness by combining liposomal honokiol with cisplatin in lung cancer model. BMC Cancer 8, 242.
Jiraviriyakul, A., Songjang, W., Kaewthet, P., Tanawatkitichai, P., Bayan, P., Pongcharoen, S., 2019. Honokiol-enhanced cytotoxic T lymphocyte activity against cholangiocarcinoma cells mediated by dendritic cells pulsed with damage-associated molecular patterns. World J. Gastroenterol. 25, 3941–3955.
Kim, I.S., Gao, Y., Welte, T., Wang, H., Liu, J., Janghorban, M., Sheng, K., Niu, Y., Goldstein, A., Zhao, N., Bado, I., Lo, H.C., Toneff, M.J., Nguyen, T., Bu, W., Jiang, W., Arnold, J., Gu, F., He, J., Jebakumar, D., Walker, K., Li, Y., Mo, Q., Westbrook, T.F., Zong, C., Rao, A., Sreekumar, A., Rosen, J.M., Zhang, X.H., 2019. Immuno-subtyping of breast cancer reveals distinct myeloid cell profiles and immunotherapy resistance mechanisms. Nat. Cell Biol. 21, 1113–1126.
Klingensmith, N.J., Chen, C.W., Liang, Z., Burd, E.M., Farris, A.B., Arbiser, J.L., Ford, M. L., Coopersmith, C.M., 2018. Honokiol increases CD4+ T cell activation and decreases TNF but fails to improve survival following sepsis. Shock 50, 178–186.
Leeman-Neill, R.J., Cai, Q., Joyce, S.C., Thomas, S.M., Bhola, N.E., Neill, D.B., Arbiser, J. L., Grandis, J.R., 2010. Honokiol inhibits epidermal growth factor receptor signaling and enhances the antitumor effects of epidermal growth factor receptor inhibitors. Clin. Cancer Res. 16, 2571–2579.
Li, Q., Cheng, Y., Zhang, Z., Bi, Z., Ma, X., Wei, Y., Wei, X., 2022a. Inhibition of ROCK ameliorates pulmonary fibrosis by suppressing M2 macrophage polarisation through phosphorylation of STAT3. Clin. Transl. Med. 12, e1036.
Li, S., Chen, J., Fan, Y., Wang, C., Wang, C., Zheng, X., Chen, F., Li, W., 2022b. Liposomal Honokiol induces ROS-mediated apoptosis via regulation of ERK/p38-MAPK signaling and autophagic inhibition in human medulloblastoma. Signal. Transduct. Target. Ther. 7, 49.
Li, S., Li, L., Chen, J., Fan, Y., Wang, C., Du, Y., Guo, C., Chen, F., Li, W., 2021. Liposomal honokiol inhibits glioblastoma growth through regulating macrophage polarization. Ann. Transl. Med. 9, 1644.
Li, Z., Liu, Y., Zhao, X., Pan, X., Yin, R., Huang, C., Chen, L., Wei, Y., 2008. Honokiol, a natural therapeutic candidate, induces apoptosis and inhibits angiogenesis of ovarian tumor cells. Eur. J. Obstet. Gynecol. Reprod. Biol. 140, 95–102.
Lin, C.J., Chen, T.L., Tseng, Y.Y., Wu, G.J., Hsieh, M.H., Lin, Y.W., Chen, R.M., 2016. Honokiol induces autophagic cell death in malignant glioma through reactive oxygen species-mediated regulation of the p53/PI3K/Akt/mTOR signaling pathway. Toxicol. Appl. Pharmacol. 304, 59–69.
Liu, X., Zhang, W., Xu, Y., Xu, X., Jiang, Q., Ruan, J., Wu, Y., Zhou, Y., Saw, P.E., Luo, B., 2022. Targeting PI3Kgamma/AKT pathway remodels LC3-associated phagocytosis induced immunosuppression after radiofrequency ablation. Adv. Sci. (Weinh) 9, e2102182.
Loeuillard, E., Yang, J., Buckarma, E., Wang, J., Liu, Y., Conboy, C., Pavelko, K.D., Li, Y., O'Brien, D., Wang, C., Graham, R.P., Smoot, R.L., Dong, H., Ilyas, S., 2020. Targeting tumor-associated macrophages and granulocytic myeloid-derived suppressor cells augments PD-1 blockade in cholangiocarcinoma. J. Clin. Invest. 130, 5380–5396.
Lu, C., Redd, P.S., Lee, J.R., Savage, N., Liu, K., 2016. The expression profiles and regulation of PD-L1 in tumor-induced myeloid-derived suppressor cells. Oncoimmunology 5, e1247135.
Luo, H., Zhong, Q., Chen, L.J., Qi, X.R., Fu, A.F., Yang, H.S., Yang, F., Lin, H.G., Wei, Y. Q., Zhao, X., 2008. Liposomal honokiol, a promising agent for treatment of cisplatin-resistant human ovarian cancer. J. Cancer Res. Clin. Oncol. 134, 937–945.
Ma, L., Chen, J., Wang, X., Liang, X., Luo, Y., Zhu, W., Wang, T., Peng, M., Li, S., Jie, S., Peng, A., Wei, Y., Chen, L., 2011. Structural modification of honokiol, a biphenyl occurring in Magnolia officinalis: the evaluation of honokiol analogues as inhibitors of angiogenesis and for their cytotoxicity and structure-activity relationship. J. Med. Chem. 54, 6469–6481.
Ma, Q., Xu, M., Jing, X., Qiu, J., Huang, S., Yan, H., Yin, L., Lou, J., Zhao, L., Fan, Y., Qiu, P., 2023. Honokiol suppresses the aberrant interactions between renal resident macrophages and tubular epithelial cells in lupus nephritis through the NLRP3/IL-33/ST2 axis. Cell Death. Dis. 14, 174.
Mann, J., 2002. Natural products in cancer chemotherapy: past, present and future. Nat. Rev. Cancer 2, 143–148.
Mihara, T., Mikawa, S., Kaji, N., Endo, M., Oikawa, T., Tong-Rong, J., Ozaki, H., Hori, M., 2017. Therapeutic action of honokiol on postoperative ileus via downregulation of iNOS gene expression. Inflammation 40, 1331–1341.
Morad, G., Helmink, B.A., Sharma, P., Wargo, J.A., 2021. Hallmarks of response, resistance, and toxicity to immune checkpoint blockade. Cell 184, 5309–5337.
Nam, S., Lee, A., Lim, J., Lim, J.S., 2019. Analysis of the expression and regulation of PD-1 protein on the surface of myeloid-derived suppressor cells (MDSCs). Biomol. Ther. (Seoul) 27, 63–70.
Prasad, R., Singh, T., Katiyar, S.K., 2017. Honokiol inhibits ultraviolet radiation-induced immunosuppression through inhibition of ultraviolet-induced inflammation and DNA hypermethylation in mouse skin. Sci. Rep. 7, 1657.
Rauf, A., Olatunde, A., Imran, M., Alhumaydhi, F.A., Aljohani, A.S.M., Khan, S.A., Uddin, M.S., Mitra, S., Emran, T.B., Khayrullin, M., Rebezov, M., Kamal, M.A., Shariati, M.A., 2021. Honokiol: a review of its pharmacological potential and therapeutic insights. Phytomedicine 90, 153647.
Reck, M., Remon, J., Hellmann, M.D., 2022. First-Line Immunotherapy for Non-Small-Cell Lung Cancer. J. Clin. Oncol. 40, 586–597.
Retseck, J., Nasr, A., Lin, Y., Lin, H., Mendiratta, P., Butterfield, L.H., Tarhini, A.A., 2018. Long term impact of CTLA4 blockade immunotherapy on regulatory and effector immune responses in patients with melanoma. J. Transl. Med. 16, 184.
Rodell, C.B., Arlauckas, S.P., Cuccarese, M.F., Garris, C.S., Li, R., Ahmed, M.S., Kohler, R. H., Pittet, M.J., Weissleder, R., 2018. TLR7/8-agonist-loaded nanoparticles promote the polarization of tumour-associated macrophages to enhance cancer immunotherapy. Nat Biomed Eng 2, 578–588.
Song, J.M., Anandharaj, A., Upadhyaya, P., Kirtane, A.R., Kim, J.H., Hong, K.H., Panyam, J., Kassie, F., 2016. Honokiol suppresses lung tumorigenesis by targeting EGFR and its downstream effectors. Oncotarget 7, 57752–57769.
Strauss, L., Mahmoud, M.A.A., Weaver, J.D., Tijaro-Ovalle, N.M., Christofides, A., Wang, Q., Pal, R., Yuan, M., Asara, J., Patsoukis, N., Boussiotis, V.A., 2020. Targeted deletion of PD-1 in myeloid cells induces antitumor immunity. Sci. Immunol. 5.
Sung, H., Ferlay, J., Siegel, R.L., Laversanne, M., Soerjomataram, I., Jemal, A., Bray, F., 2021. Global cancer statistics 2020: GLOBOCAN estimates of incidence and mortality worldwide for 36 cancers in 185 countries. CA Cancer J. Clin. 71, 209–249.
Vergadi, E., Ieronymaki, E., Lyroni, K., Vaporidi, K., Tsatsanis, C., 2017. Akt signaling pathway in macrophage activation and M1/M2 polarization. J. Immunol. 198, 1006–1014.
Waldman, A.D., Fritz, J.M., Lenardo, M.J., 2020. A guide to cancer immunotherapy: from T cell basic science to clinical practice. Nat. Rev. Immunol. 20, 651–668.
Wang, X.H., Cai, L.L., Zhang, X.Y., Deng, L.Y., Zheng, H., Deng, C.Y., Wen, J.L., Zhao, X., Wei, Y.Q., Chen, L.J., 2011. Improved solubility and pharmacokinetics of PEGylated liposomal honokiol and human plasma protein binding ability of honokiol. Int. J. Pharm. 410, 169–174.
Wei, S.C., Levine, J.H., Cogdill, A.P., Zhao, Y., Anang, N.A.S., Andrews, M.C., Sharma, P., Wang, J., Wargo, J.A., Pe'er, D., Allison, J.P., 2017. Distinct Cellular Mechanisms Underlie Anti-CTLA-4 and Anti-PD-1 Checkpoint Blockade. Cell 170, 1120–1133 e1117.
Weisser, S.B., McLarren, K.W., Voglmaier, N., van Netten-Thomas, C.J., Antov, A., Flavell, R.A., Sly, L.M., 2011. Alternative activation of macrophages by IL-4 requires SHIP degradation. Eur. J. Immunol. 41, 1742–1753.
Wen, J., Fu, A.F., Chen, L.J., Xie, X.J., Yang, G.L., Chen, X.C., Wang, Y.S., Li, J., Chen, P., Tang, M.H., Shao, X.M., Lu, Y., Zhao, X., Wei, Y.Q., 2009. Liposomal honokiol inhibits VEGF-D-induced lymphangiogenesis and metastasis in xenograft tumor model. Int. J. Cancer 124, 2709–2718.
Wu, W., Tang, M.H., Tang, H., Chen, K., Fu, J., Wang, L., Xue, L.L., Peng, A., Ye, H., Chen, L.J., 2018. Identification, characterization and HPLC quantification of

formulation-related impurities of honokiol, an antitumor natural drug candidate in clinical trials. J. Pharm. Biomed. Anal. 153, 186–192.
Xin Yu, J., Hubbard-Lucey, V.M., Tang, J., 2019. Immuno-oncology drug development goes global. Nat. Rev. Drug Discov. 18, 899–900.
Xue, J., Schmidt, S.V., Sander, J., Draffehn, A., Krebs, W., Quester, I., De Nardo, D., Gohel, T.D., Emde, M., Schmidleithner, L., Ganesan, H., Nino-Castro, A., Mallmann, M.R., Labzin, L., Theis, H., Kraut, M., Beyer, M., Latz, E., Freeman, T.C., Ulas, T., Schultze, J.L., 2014. Transcriptome-based network analysis reveals a spectrum model of human macrophage activation. Immunity 40, 274–288.
Yang, B., Ni, X., Chen, L., Zhang, H., Ren, P., Feng, Y., Chen, Y., Fu, S., Wu, J., 2017a. Honokiol-loaded polymeric nanoparticles: an active targeting drug delivery system for the treatment of nasopharyngeal carcinoma. Drug Deliv. 24, 660–669.
Yang, J., Wu, W., Wen, J., Ye, H., Luo, H., Bai, P., Tang, M., Wang, F., Zheng, L., Yang, S., Li, W., Peng, A., Yang, L., Wan, L., Chen, L., 2017b. Liposomal honokiol induced lysosomal degradation of Hsp90 client proteins and protective autophagy in both gefitinib-sensitive and gefitinib-resistant NSCLC cells. Biomaterials 141, 188–198.
Yu, J., Green, M.D., Li, S., Sun, Y., Journey, S.N., Choi, J.E., Rizvi, S.M., Qin, A., Waninger, J.J., Lang, X., Chopra, Z., El Naqa, I., Zhou, J., Bian, Y., Jiang, L., Tezel, A., Skvarce, J., Achar, R.K., Sitto, M., Rosen, B.S., Su, F., Narayanan, S.P., Cao, X., Wei, S., Szeliga, W., Vatan, L., Mayo, C., Morgan, M.A., Schonewolf, C.A., Cuneo, K., Kryczek, I., Ma, V.T., Lao, C.D., Lawrence, T.S., Ramnath, N., Wen, F., Chinnaiyan, A.M., Cieslik, M., Alva, A., Zou, W., 2021. Liver metastasis restrains immunotherapy efficacy via macrophage-mediated T cell elimination. Nat. Med. 27, 152–164.
Zhang, Q., Raje, V., Yakovlev, V.A., Yacoub, A., Szczepanek, K., Meier, J., Derecka, M., Chen, Q., Hu, Y., Sisler, J., Hamed, H., Lesnefsky, E.J., Valerie, K., Dent, P., Larner, A.C., 2013. Mitochondrial localized Stat3 promotes breast cancer growth via phosphorylation of serine 727. J. Biol. Chem. 288, 31280–31288.
Zhao, S.J., Kong, F.Q., Jie, J., Li, Q., Liu, H., Xu, A.D., Yang, Y.Q., Jiang, B., Wang, D.D., Zhou, Z.Q., Tang, P.Y., Chen, J., Wang, Q., Zhou, Z., Chen, Q., Yin, G.Y., Zhang, H. W., Fan, J., 2020. Macrophage MSR1 promotes BMSC osteogenic differentiation and M2-like polarization by activating PI3K/AKT/GSK3beta/beta-catenin pathway. Theranostics 10, 17–35.
Zheng, H., Matte-Martone, C., Li, H., Anderson, B.E., Venketesan, S., Sheng Tan, H., Jain, D., McNiff, J., Shlomchik, W.D., 2008. Effector memory CD4+ T cells mediate graft-versus-leukemia without inducing graft-versus-host disease. Blood 111, 2476–2484.
Zheng, R., Zhang, S., Zeng, H., Wang, S., Sun, K., Chen, R., Li, L., Wei, W., He, J., 2022. Cancer incidence and mortality in China, 2016. J. National Cancer Center.
Zheng, Z., Zhang, J., Jiang, J., He, Y., Zhang, W., Mo, X., Kang, X., Xu, Q., Wang, B., Huang, Y., 2020. Remodeling tumor immune microenvironment (TIME) for glioma therapy using multi-targeting liposomal codelivery. J. Immunother. Cancer 8.
Zhou, B., Li, H., Xing, C., Ye, H., Feng, J., Wu, J., Lu, Z., Fang, J., Gao, S., 2017. Honokiol induces proteasomal degradation of AML1-ETO oncoprotein via increasing ubiquitin conjugase UbcH8 expression in leukemia. Biochem. Pharmacol. 128, 12–25.
Zhou, Y., Tang, J., Lan, J., Zhang, Y., Wang, H., Chen, Q., Kang, Y., Sun, Y., Feng, X., Wu, L., Jin, H., Chen, S., Peng, Y., 2023. Honokiol alleviated neurodegeneration by reducing oxidative stress and improving mitochondrial function in mutant SOD1 cellular and mouse models of amyotrophic lateral sclerosis. Acta Pharm Sin B 13, 577–597.
Zhu, J., Xu, S., Gao, W., Feng, J., Zhao, G., 2019a. Honokiol induces endoplasmic reticulum stress-mediated apoptosis in human lung cancer cells. Life Sci. 221, 204–211.
Zhu, Y., Yang, J., Xu, D., Gao, X.M., Zhang, Z., Hsu, J.L., Li, C.W., Lim, S.O., Sheng, Y.Y., Zhang, Y., Li, J.H., Luo, Q., Zheng, Y., Zhao, Y., Lu, L., Jia, H.L., Hung, M.C., Dong, Q.Z., Qin, L.X., 2019b. Disruption of tumour-associated macrophage trafficking by the osteopontin-induced colony-stimulating factor-1 signalling sensitises hepatocellular carcinoma to anti-PD-L1 blockade. Gut 68, 1653–1666.